Title
Structural Uncertainty in the Sensitivity of Urban Temperatures to Anthropogenic Heat Flux

Journal
Journal of Advances in Modeling Earth Systems, 16(10)

ISSN
1942-2466

Authors
Li, Dan
Sun, Ting
Yang, Jiachuan
et al.

Publication Date
2024-10-01

DOI
10.1029/2024ms004431

AGU ADVANCING EARTH AND SPACE SCIENCES

JAMES | Journal of Advances in Modeling Earth Systems®

RESEARCH ARTICLE
10.1029/2024MS004431

Key Points:

- Model choices can affect the sensitivities of urban temperatures to anthropogenic heat flux by as much as an order of magnitude
- The substantial structural uncertainty highlights the challenges associated with simplifying complex urban environments in numerical models
- The sensitivities of urban temperatures to anthropogenic heat flux seem to converge at large anthropogenic heat flux

Supporting Information:

Supporting Information may be found in the online version of this article.

Correspondence to:

D. Li,
lidan@bu.edu

Citation:

Li, D., Sun, T., Yang, J., Zhang, N., Vahmani, P., & Jones, A. (2024). Structural uncertainty in the sensitivity of urban temperatures to anthropogenic heat flux. *Journal of Advances in Modeling Earth Systems*, *16*, e2024MS004431. https://doi.org/10.1029/2024MS004431

Received 5 MAY 2024
Accepted 30 SEP 2024

Author Contributions:

Conceptualization: Dan Li, Pouya Vahmani, Andrew Jones
Data curation: Dan Li
Formal analysis: Dan Li, Ting Sun
Funding acquisition: Dan Li
Investigation: Dan Li
Methodology: Dan Li, Ting Sun, Jiachuan Yang, Ning Zhang
Resources: Dan Li
Software: Dan Li
Validation: Dan Li
Visualization: Dan Li
Writing – original draft: Dan Li

Structural Uncertainty in the Sensitivity of Urban Temperatures to Anthropogenic Heat Flux

Dan Li[1,2], Ting Sun[3], Jiachuan Yang[4], Ning Zhang[5], Pouya Vahmani[6], and Andrew Jones[6]

[1]Department of Earth and Environment, Boston University, Boston, MA, USA, [2]Department of Mechanical Engineering, Boston University, Boston, MA, USA, [3]Department of Risk and Disaster Reduction, University College London, London, UK, [4]Department of Civil and Environmental Engineering, The Hong Kong University of Science and Technology, Hong Kong, China, [5]School of Atmospheric Sciences, Nanjing University, Nanjing, China, [6]Lawrence Berkeley National Laboratory, Berkeley, CA, USA

Abstract One key source of uncertainty for weather and climate models is structural uncertainty arising from the fact that these models must simplify or approximate complex physical, chemical, and biological processes that occur in the real world. However, structural uncertainty is rarely examined in the context of simulated effects of anthropogenic heat flux in cities. Using the Weather Research and Forecasting (WRF) model coupled with a single-layer urban canopy model, it is found that the sensitivity of urban canopy air temperature to anthropogenic heat flux can differ by an order of magnitude depending on how anthropogenic heat flux is released to the urban environment. Moreover, varying model structures through changing the treatment of roof-air interaction and the parameterization of convective heat transfer between the canopy air and the atmosphere can affect the sensitivity of urban canopy air temperature by a factor of 4. Urban surface temperature and 2-m air temperature are less sensitive to the methods of anthropogenic heat flux release and the examined model structural variants than urban canopy air temperature, but their sensitivities to anthropogenic heat flux can still vary by as much as a factor of 4 for surface temperature and 2 for 2-m air temperature. Our study recommends using temperature sensitivity instead of temperature response to understand how various physical processes (and their representations in numerical models) modulate the simulated effects of anthropogenic heat flux.

Plain Language Summary Numerical models are often used to simulate the effects of anthropogenic heat flux, which is generated by human activities such as building energy consumption, transportation, etc. These models inevitably have structural uncertainties because they simplify the real world; hence, the simulated effects of anthropogenic heat flux also possess structural uncertainties. Yet, the structural uncertainties associated with the simulated effects of anthropogenic heat flux have not been studied before. In this study, we quantify such structural uncertainties using a suite of simulations conducted with the Weather Research and Forecasting (WRF) model. Using the sensitivity of urban temperatures to anthropogenic heat flux as the metric, we find that different urban temperatures show different sensitivities to anthropogenic heat flux and these sensitivities can vary by as large as an order of magnitude depending on the anthropogenic heat flux release methods and key model structural choices.

1. Introduction

More than 50% of the global population now lives in cities, which requires numerical weather prediction models (F. Chen et al., 2011) and sometimes global climate/earth system models (Li et al., 2016a, 2016b; Oleson & Feddema, 2020; Oleson et al., 2008) to provide urban meteorological information. These urbanized weather and climate models are also used to study how the simulated urban climate responds to various forcing or perturbations. In this work, we focus on how numerical model simulated urban temperatures vary with anthropogenic heat flux (Q_{AH}), which represents heat generated by human activities such as building energy consumption, transportation, metabolism, and so on (Oke et al., 2017).

Much of the research from the urban climate community focuses on quantifying the magnitude of anthropogenic heat flux (see a review by Sailor (2011) and also Sailor et al. (2015)). Nowadays many global scale data sets of anthropogenic heat flux are available (e.g., Allen et al., 2011; Dong et al., 2017; Varquez et al., 2021). However, of equal importance is to quantify the sensitivity of urban temperature (T) to anthropogenic heat flux because

Writing – review & editing: Dan Li, Ting Sun, Jiachuan Yang, Ning Zhang, Pouya Vahmani, Andrew Jones

$$\Delta T = \frac{dT}{dQ_{AH}} \Delta Q_{AH}. \quad (1)$$

Here ΔQ_{AH} is a change (Δ) in the magnitude of Q_{AH} (e.g., from no Q_{AH} to a positive value of Q_{AH}) and represents a forcing to the urban system, dT/dQ_{AH} is the temperature sensitivity to Q_{AH}, and ΔT is the temperature response to ΔQ_{AH}.

Previous work often used numerical models to quantify ΔT in response to ΔQ_{AH} (see a review by Wang et al. (2023)). Numerical modeling was the primary tool for such tasks because in observations it is difficult to separate Q_{AH} from other heat fluxes such as sensible heat flux and concomitantly their influences on surface climates. Previous modeling studies, nonetheless, tend to focus on ΔT, which depends on the magnitude of ΔQ_{AH} as can be seen from Equation 1. Wang et al. (2023) argued that the sensitivity (dT/dQ_{AH}), or $\Delta T/\Delta Q_{AH}$, is a better index to compare across studies since it partly removes the effect of varying ΔQ_{AH} in different studies. They reported that dT/dQ_{AH} shows some consistency across different modeling studies that used different numerical models, examined different cities, and had different ΔQ_{AH} values, with a rule-of-thumb value of about 0.01 K/(W m^{-2}). Wang et al. (2023) further developed a forcing-feedback framework to diagnose the physical processes that control the spatial and temporal variability of dT_C/dQ_{AH} across the Contiguous United States, where T_C refers to the urban canopy air temperature. They found that the spatio-temporal variability of dT_C/dQ_{AH} was predominately caused by the variability of convective heat transfer coefficient between the canopy air and the atmosphere above the urban canopy.

Building on the work by Wang et al. (2023), this study also focuses on dT/dQ_{AH} but aims to address the structural uncertainty associated with dT/dQ_{AH}, a topic previously unexplored. Urban land surface models used for weather and climate simulations simplify the intricate, three-dimensional urban environment and its heterogeneous emissions of Q_{AH}. The abstraction of the urban environment can be structured in multiple legitimate ways (Lipson et al., 2024). However, most existing studies, including the study by Wang et al. (2023), have relied on a single urban model, thereby failing to consider the structural uncertainty associated with dT/dQ_{AH}. To examine the structural uncertainty associated with dT/dQ_{AH}, one might employ multiple urban models to explore how dT/dQ_{AH} varies among them. However, this approach introduces interpretive challenges due to the inherent differences among models. To circumvent this issue, we adopt a single urban model and systematically vary key structural elements and the methods by which Q_{AH} is released into the urban environment. This approach allows us to dissect, step by step, the impacts of these variations (as well as the physical processes that they represent) on dT/dQ_{AH}. Although our approach does not encompass every possible model configuration, it does replicate the structure of prominent existing models, providing a systematic framework for understanding the consequences of specific model choices on dT/dQ_{AH}.

This study further addresses several key remaining questions related to dT/dQ_{AH} that were not investigated by Wang et al. (2023). Wang et al. (2023) used land-only simulations and thus ignored atmospheric feedback. They recommended that atmospheric feedback should be addressed in follow-up studies. Moreover, they used a single urban temperature variable, the canopy air temperature (T_C). In this study, we fill these two research gaps by using (a) land-atmosphere coupled simulations and (b) multiple temperature variables (including the widely used 2-m air temperature T_2 and surface temperature T_S, in addition to the canopy air temperature T_C). T_C may be viewed as the temperature within the urban canyon but is less studied since it is typically not a standard output of weather and climate models. On the other hand, T_2 is a more widely used air temperature variable as it is a standard output, but its interpretation over urban environment is challenging (see the discussion in the supplementary materials of Qin et al. (2023)). In short, T_2 is the air temperature at 2 m above the displacement height and hence does not represent the air temperature at 2 m above the urban canyon floor. T_S is a surface temperature, but it does not represent the surface temperature of a single urban facet (e.g., roof or wall). Given the heterogeneity of urban environment even in abstract urban models, it represents an aggregated surface temperature for the entire urban grid cell with the aggregation not entirely based on geometry.

The paper is structured as follows: Section 2 provides detailed descriptions of the numerical model and the simulations; the results are then presented in Section 3; Section 4 concludes this study with a summary and discussions of the implications of this work.

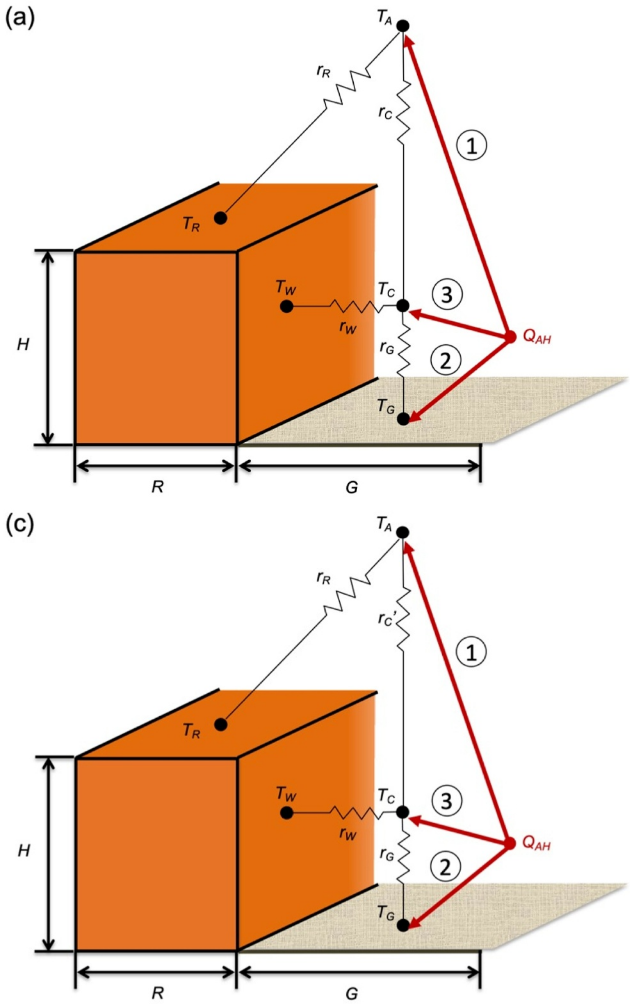

Figure 1. A schematic of four structural variants (SV) of single-layer urban canopy model (SLUCM) (panels a–d) and three Q_{AH} release methods (indicated by 1–3 on each panel). (a) SV 1: the default WRF-SLUCM structure; (b) SV 2: a CLMU (Community Land Model—Urban)-like structure where the roof interacts with the canopy air instead of with the atmosphere directly; (c) SV 3: the default SLUCM structure but r_C is computed with the momentum roughness length (denoted as r_C'); (d) SV 4: a CLMU-like structure and r_C is computed with the momentum roughness length (denoted as r_C'). In this figure, T is temperature and r is the resistance for heat transfer, and the subscripts A, R, W, C, G represent atmosphere, roof, wall, canopy air, and canyon ground, respectively. H, R, G represent the building height, the roof width, and the canyon width, respectively. Q_{AH} is a prescribed input that supposedly represents the total anthropogenic heat flux from all sources.

2. Methodology and Data

2.1. WRF-SLUCM

This study uses the Weather Research and Forecasting (WRF) model version 4.2.2 (Skamarock et al., 2019). For the land surface component, we use the Noah land surface model coupled with a single-layer urban canopy model (SLUCM) (Kusaka et al., 2001) but without the mosaic approach (Li et al., 2013). This modeling system will be called WRF-SLUCM hereafter (F. Chen et al., 2011). For each grid cell that is classified as an urban grid cell, WRF-SLUCM treats the grid cell as a combination of an impervious part (handled by the SLUCM) and a pervious part (handled by the Noah land surface model).

Figure 1a shows a schematic of the SLUCM. As can be seen, the SLUCM is designed based on the concept of a two-dimensional urban canyon and models the roof, the walls, and the canyon ground. These impervious urban surfaces will be called urban facets hereafter. The walls and the canyon ground interact with the atmosphere through the canopy air while the roof directly interacts with the atmosphere. All temperature variables (T_A, T_R, T_C, T_W, T_G, where the subscripts A, R, C, W, G represent atmosphere, roof, canopy air, wall, and canyon ground, respectively) shown in Figure 1a are prognostic temperatures in the sense that they are computed based on energy balance principles and any changes in these variables at one time step will affect model results in the following time steps. In the first part of this study, we will focus on the sensitivity of T_C to Q_{AH}, or dT_C/dQ_{AH}. In the second part of this study, we will examine the sensitivities of the widely used surface temperature (T_S) and 2-m air temperature (T_2), both of which can be viewed as diagnostic variables from the perspective of the land model. The definitions and computation of T_S and T_2 will be explained later.

2.2. The Sensitivity of T_C to Q_{AH}

2.2.1. Q_{AH} Release Methods

As WRF-SLUCM does not explicitly model the building interior, Q_{AH} needs to be prescribed, which is often based on inventory data or outputs of building energy models (e.g., F. Chen et al., 2016; L. Chen et al., 2024; Luo et al., 2020; Vahmani et al., 2022; Yang et al., 2019). Within the confines of the current WRF-SLUCM, there are at least three methods of releasing Q_{AH} into the urban environment, indicated by 1, 2, 3 in Figure 1. The first method releases Q_{AH} directly to the upper atmosphere. This is the default option in WRF-SLUCM, which is accomplished by aggregating Q_{AH} with the traditional sensible heat flux. The second method treats Q_{AH} as an additional energy source in the surface energy budget of canyon ground. The third method incorporates Q_{AH} into the energy budget of canopy air. We implement the latter two methods into WRF-SLUCM to test how dT/dQ_{AH} varies with the Q_{AH} release methods. The latter two methods are motivated by other models and/or previous studies. For example, the default Community Land Model - Urban (CLMU) and the Met Office—Reading Urban Surface Exchange Scheme (Bohnenstengel et al., 2014) use the second method. The study by Wang et al. (2023) used the third approach.

2.2.2. Structural Variants of SLUCM

In addition to examining the structural uncertainty associated with dT/dQ_{AH} through the lens of how Q_{AH} is released, we also examine the uncertainty introduced by different structural variants (SV) of SLUCM.

1. SV 1: linking roof with the atmosphere

In SV 1 (i.e., the default WRF-SLUCM structure), the roof communicates with the atmosphere and thus does not directly affect the canopy air, which is defined over the canyon part. WRF-SLUCM (and many other UCMs) assumes that the canopy air has zero heat capacity and thus the canopy air energy budget simplifies to

$$Q_W(2H) + Q_G G + Q_{AH}(R+G)\delta_{3i} = Q_C G, \tag{2}$$

where H is the building height, G is the canyon width, and R is the roof width (see Figure 1a). $Q_W = C_a(T_W - T_C)/r_W$ is sensible heat flux from the wall to the canopy air; C_a is the volumetric heat capacity of air (J m^{-3} K^{-1}); r_W is the convective heat transfer resistance between the wall and the canopy air (s m^{-1}); $2H$ represents the areas over which the wall sensible heat flux is generated (i.e., for each canyon there are two walls). Similarly, $Q_G = C_a(T_G - T_C)/r_G$ is sensible heat flux from the canyon ground to the canopy air, and $Q_C = C_a(T_C - T_A)/r_C$ is sensible heat flux from the canopy air to the atmosphere above the canopy. r_G is the convective heat transfer resistance between the ground and the canopy air (s m^{-1}), while r_C is the convective heat transfer resistance between the canopy air and the atmosphere (s m^{-1}). It is important to point out that Q_{AH} has to be multiplied by $(R+G)$ since Q_{AH} is defined over the entire impervious land in WRF-SLUCM, which includes both roof and canyon. δ_{ij} is the Kronecker delta and is equal to 1 when $i=j$ and 0 otherwise. Here i indicates the Q_{AH} release method as shown in Figure 1a and δ_{3i} in Equation 2 implies that Q_{AH} is only considered in the canopy air energy budget by method 3. Similarly, δ_{1i} and δ_{2i} should appear in the budget equations for air temperature and ground temperature, which are nonetheless not provided here for simplicity.

For completeness, we define Q_R here, which is sensible heat flux from the roof surface to the atmosphere. It is computed following $Q_R = C_a(T_R - T_A)/r_R$. One can see that in this SV Q_R is not directly related to T_C.

Substituting the expressions for Q_W, Q_G, and Q_C into Equation 2 yields

$$T_C = \frac{\frac{2H}{r_W}T_W + \frac{G}{r_G}T_G + \frac{G}{r_C}T_A + (R+G)\frac{Q_{AH}}{C_a}\delta_{3i}}{\frac{2H}{r_W} + \frac{G}{r_G} + \frac{G}{r_C}}. \tag{3}$$

2. SV 2: linking roof with canopy air

While the default WRF-SLUCM parameterizes the roof-air interaction in a way that the roof directly interacts with the atmosphere (see Figure 1a), other urban canopy models such as CLMU connects the roof to the canopy air (see Figure 1b). These two SVs represent two extremes. In SV 1 (Figure 1a), the roof is treated independently from the canyon, which includes the walls and the canyon ground; while in SV 2 (Figure 1b), any fluxes from the roof are completely mixed with those from the walls/ground within the canopy air. In reality, the roof-air interaction is probably somewhere in between these two extremes depending on the integration power of turbulence within and above the urban canyon. Hence, studying these two extremes can help constrain the range of urban temperature sensitivities to Q_{AH} due to uncertainties related to the treatment of roof-air interaction.

With a CLMU-like structure (Figure 1b), it is important to recognize that the energy budget for the canopy air now changes to

$$Q_R R + Q_W(2H) + Q_G G + Q_{AH}(R+G)\delta_{3i} = Q_C(R+G). \tag{4}$$

Here $Q_R = C_a(T_R - T_C)/r_R$ is sensible heat flux from the roof surface to the canopy air. Note that Q_R is now related to the temperature difference between T_R and T_C, instead of the temperature difference between T_R and T_A as in SV 1. As a result, the parameterization of r_R is also adjusted in SV 2 so that it is identical to r_W and r_G, following CLMU. Also note that Q_C now must be multiplied by $(R+G)$ because the canopy air is implicitly assumed to be distributed over both the roof and the canyon. This is in contrast with the previous budget equation (Equation 2) where Q_C is multiplied by G because the canopy air is implicitly assumed to only exist over the canyon. This change has important implications for dT_C/dQ_{AH}, as shall be seen later.

In this SV, we can derive

$$T_C = \frac{\frac{R}{r_R}T_R + \frac{2H}{r_W}T_W + \frac{G}{r_G}T_G + \frac{R+G}{r_C}T_A + (R+G)\frac{Q_{AH}}{C_a}\delta_{3i}}{\frac{R}{r_R} + \frac{2H}{r_W} + \frac{G}{r_G} + \frac{R+G}{r_C}}. \tag{5}$$

3. SV 3: computing r_C with the momentum roughness length

Wang et al. (2023) showed that the convective heat transfer coefficient (or equivalently r_C) is the most important parameter in controlling the spatio-temporal variability of dT_C/dQ_{AH}. Currently, the parameterization of r_C remains a challenge. This study does not address the theoretical deficiency of relying on Monin-Obukhov similarity theory (Monin & Obukhov, 1954) to parameterize r_C for urban canopies. Instead, we examine how dT_C/dQ_{AH} varies with certain choices within the confines of the current parameterization for r_C. More specifically, whether the momentum roughness length or the thermal roughness length is used to compute r_C is examined here.

In SV 1, r_C is computed following Equation 6 below when buoyancy effects are ignored:

$$r_C = \frac{\ln\left(\frac{z_A}{z_{0h}}\right)}{\kappa u_*}, \tag{6}$$

where κ is the von-Karman constant, u_* is the friction velocity, z_A is the height of the lowest atmospheric model level (i.e., where T_A is defined) relative to the displacement height, z_{0h} is the thermal roughness length. In this SV, T_C is effectively defined at z_{0h} above the displacement height on the extrapolated atmospheric surface layer temperature profile. Note that in the WRF-SLUCM model, the buoyancy effects are considered but they are not shown here for simplicity.

In SV 3, the calculation of r_C is similar to Equation 6 but with the momentum roughness length (z_0) replacing the thermal roughness length (z_{0h}). To make it clear, we denote this new r_C as r'_C on Figure 1c, which is computed as

$$r'_C = \frac{\ln\left(\frac{z_A}{z_0}\right)}{\kappa u_*}. \tag{7}$$

Effectively, T_C is defined at z_0 above the displacement height in SV 3.

For a completely homogeneous rough surface where the radiative surface temperature is used to calculate sensible heat flux, the thermal roughness length should be used to calculate the heat transfer resistance (Brutsaert, 1982; Kustas et al., 1989). The resistance computed with the thermal roughness length includes both turbulent and quasi-laminar boundary layer (or sometimes called additional aerodynamic or excess) resistances (Monteith & Unsworth, 2013; Thom, 1972). The laminar boundary layer/additional aerodynamic/excess resistance arises from the fact that momentum transfer is greatly enhanced by pressure drag for rough surfaces, yet scalar transfer (including heat transfer) is not. Hence, scalar transfer effectively experiences a stronger resistance than its momentum counterpart (i.e., $r_C > r'_C$), which implies $z_{0h} < z_0$. On the extrapolated atmospheric surface layer temperature profile, the radiative surface temperature is effectively defined at the thermal roughness length above the displacement height, which is different from the aerodynamic surface temperature often defined at the momentum roughness length above the displacement height (Chehbouni et al., 1996; Troufleau et al., 1997).

While the theory has been reasonably well established for land-atmosphere interaction over a homogeneous surface (Brutsaert, 1982; Monteith & Unsworth, 2013), it remains unclear whether z_0 or z_{0h} should be used to compute r_C in urban canopy models. Different models deal with this aspect differently. For example, the WRF-SLUCM (as well as other urban canopy models such as the Town Energy Balance model (Masson, 2000) and the Geophysical Fluid Dynamics Laboratory Urban Canopy Model (Li et al., 2016a, 2016b)) uses the thermal roughness length to compute r_C. Nonetheless, one could argue that the additional aerodynamic resistance has been implicitly accounted for by r_W and r_G. This is why models like CLMU uses the momentum rough length to compute r_C (in fact CLM does this for both urban and vegetated canopies) (Oleson et al., 2010). The studies by Lemonsu et al. (2004) and Li et al. (2016a) also found that using the momentum roughness length instead of the thermal roughness length to compute r_C results in T_C values that are in better agreement with observations.

4. SV4: the combination of SVs 2 and 3

We also investigate a SV that changes the roof-air interaction and the computation of r_C simultaneously, see Figure 1d (hereafter SV 4). Since both features are CLMU-like, we hypothesize that the results from SV 4 would be closer to the results from CLMU presented in Wang et al. (2023) than the other SVs.

2.3. The Sensitivities of T_S and T_2 to Q_{AH}

Figure 2 shows a schematic of how T_S and T_2 are computed by WRF-SLUCM. Note that the schematic only applies to the Noah land surface model that does not invoke the mosaic approach. The mosaic approach (and other land surface models such as the Noah-MP model) has slightly different ways of diagnosing T_S and T_2 over urban grid cells. As alluded earlier, WRF treats each urban grid cell as a combination of an impervious part (with a fraction of f_{urban}) and a pervious part (with a fraction of $1 - f_{urban}$). The pervious part is treated as grass. Hence, compared to Figure 1, the additional prognostic temperature variable is the grass surface temperature T_{GRASS}, whose calculation depends on r_{GRASS}, the resistance to heat transfer between the grass surface and the atmosphere.

WRF-SLUCM constructs a grid-cell surface temperature (T_S) following

$$T_S = (1 - f_{urban})\,T_{GRASS} + f_{urban} T_U. \tag{8}$$

However, one can see from Figures 1 and 2 that there is no prognostic temperature variable called T_U where the subscript U indicates the entire impervious land. An initial, intuitive approach might define T_U as the area-averaged surface temperatures of all impervious facets. However, within the framework of WRF-SLUCM, T_U is *not* determined by such a straightforward method. Instead, the relationship between T_U and the surface temperatures of impervious facets, such as T_G and T_W, involves a more intricate calculation than simple area-averaging. Specifically, WRF-SLUCM diagnoses T_U through

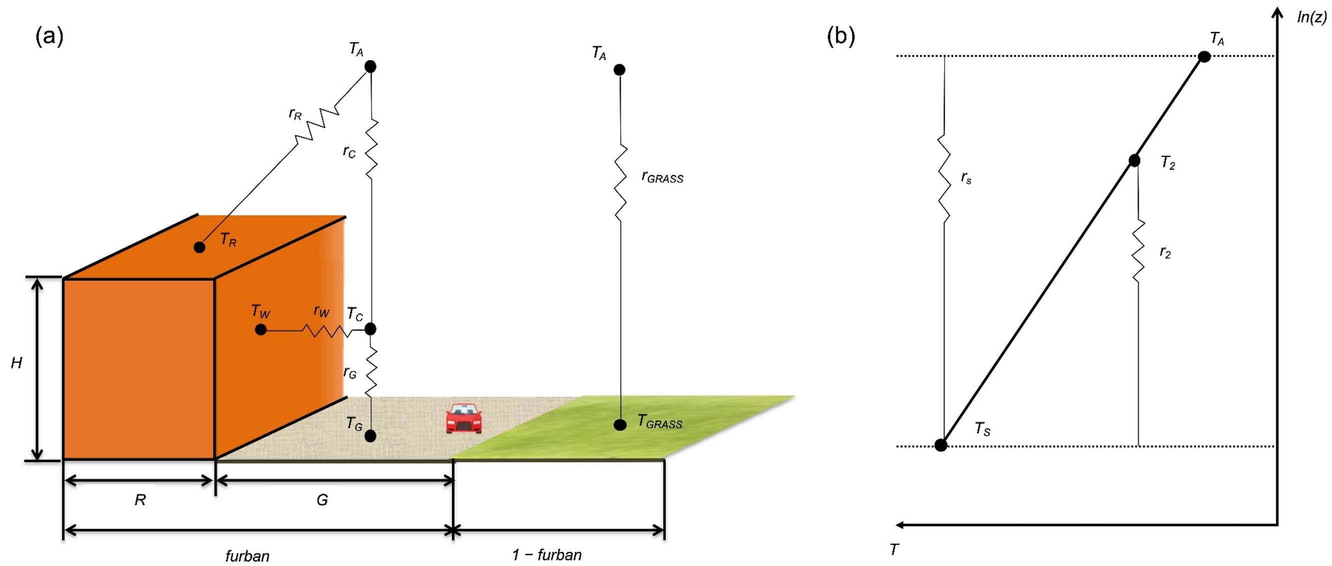

Figure 2. A schematic for T_S and T_2 calculation. (a) Weather Research and Forecasting treats each urban grid cell as a combination of an impervious part (with a fraction of f_{urban}) and a pervious or grass part (with a fraction of $1 - f_{urban}$). Here the default single-layer urban canopy model structure (see Figure 1a) is shown for the impervious part but the other SVs can be also used. The total sensible heat flux from this urban grid cell is the area-averaged sensible heat fluxes from both the impervious and pervious surfaces (see Equation 13). Similarly, the equivalent surface temperature T_S of this urban grid cell is the area-averaged surface temperatures of both the impervious and pervious surfaces (Equation 8). However, the equivalent impervious surface temperature T_U is *not* the area-averaged surface temperatures of all impervious facets, but is constructed so that the sensible heat flux caused by the temperature difference between T_U and T_A matches the total sensible heat flux from the entire impervious land (including roof, walls, and impervious ground), see Equation 9. (b) The constant-flux layer leads to a logarithmic profile for temperature within the surface layer under neutral conditions. Under thermally stratified conditions, the logarithmic profile would be modified according to Monin-Obukhov similarity theory. On this temperature profile, T_2 is defined at 2 m above the displacement height and can be viewed as an interpolation between T_S and T_A (see Equation 14).

$$Q_U = \frac{C_a(T_U - T_A)}{r_U}, \tag{9}$$

where r_U is a representative heat transfer resistance between the entire impervious land and the atmosphere and Q_U is the aggregated (correctly accounting for the surface area) sensible heat flux from the entire impervious land. The calculation of Q_U and its dependence on surface temperatures of impervious facets (such as T_G and T_W) differs among SVs.

In SVs 1 and 3, Q_U is computed as

$$Q_U = Q_R\frac{R}{R+G} + Q_C\frac{G}{R+G} = Q_R\frac{R}{R+G} + Q_W\frac{2H}{R+G} + Q_G\frac{G}{R+G} + Q_{AH}\delta_{3i}. \tag{10}$$

The term $Q_{AH}\delta_{3i}$ arises because it is part of Q_C for method 3. The sensible heat fluxes from various urban facets (Q_R, Q_W, Q_G) can be further linked to the surface temperatures of urban facets, the atmospheric temperature, and the canopy air temperature (see their definitions below Equation 2). This is how T_U is related to the surface temperatures of urban facets such as T_G.

In SVs 2 and 4, Q_U is computed as

$$Q_U = Q_C = Q_R\frac{R}{R+G} + Q_W\frac{2H}{R+G} + Q_G\frac{G}{R+G} + Q_{AH}\delta_{3i}. \tag{11}$$

Comparing Equation 11 to Equation 10 reveals that the final equation form is identical. This is because Q_U is simply an area-averaged flux over the entire impervious land. However, the definition of Q_R and the calculation of T_C are different in SVs 2 and 4 compared to SVs 1 and 3.

10.1029/2024MS004431

Combining Equations 8 and 9 yields a formulation for T_S that depends on the sensible heat flux from the entire impervious land (Q_U), the heat transfer resistance between the entire impervious land and the atmosphere (r_U), the grass surface temperature (T_{GRASS}), and the impervious surface fraction $\left(f_{urban}\right)$, as follows:

$$T_S = \left(1 - f_{urban}\right) T_{GRASS} + f_{urban}\left(\frac{Q_U}{C_a} r_U + T_A\right). \tag{12}$$

Before we discuss the calculation of 2-m air temperature, it is important to note that the grid-cell sensible heat flux (Q_S) is computed in a similar way as Equation 8, as follows:

$$Q_S = \left(1 - f_{urban}\right) Q_{GRASS} + f_{urban} Q_U. \tag{13}$$

With the grid-cell sensible heat flux in mind, the 2-m air temperature can be interpolated from T_S and T_A (see Figure 2b) using the constant-flux layer assumption, as follows:

$$Q_S = \frac{C_a (T_S - T_A)}{r_S} = \frac{C_a (T_S - T_2)}{r_2}, \tag{14}$$

where r_S is the resistance to heat transfer between the height at which the surface temperature T_S is defined and the atmosphere, while r_2 is the resistance to heat transfer between the height at which the surface temperature T_S is defined and the 2 m height (see Figure 2b). These heights are measured relative to the displacement height and hence 2 m does not represent the level of 2 m above the canyon ground. The challenges associated with interpreting T_2 over tall canopies (such as urban canopies) have been discussed elsewhere (Qin et al., 2023).

Combining Equations 13 and 14 gives

$$T_2 = T_S - \frac{\left(1 - f_{urban}\right) Q_{GRASS} + f_{urban} Q_U}{C_a} r_2. \tag{15}$$

2.4. Numerical Simulations

We conduct several simulations over the greater Boston area. Each simulation consists of 3 domains with spatial resolutions of 9, 3, and 1 km. The default WRF static data sets are used for topography (see Figure 3a), soil types, etc. In terms of land use and land cover, the NLCD40 data set (which is a combination of National Land Cover Data or NLCD and Moderate Resolution Imaging Spectroradiometer or MODIS but with NLCD taking priority) provided by WRF is used (see Figure 3b which shows the land use in the innermost domain with the classification scheme provided in Table S1 in Supporting Information S1). Since NLCD are available everywhere in the US and our domains are within the US, the land use data used in our simulations are primarily from NLCD, not MODIS. The impervious surface fraction $\left(f_{urban}\right)$ is also from NLCD, as shown in Figure 3c. In WRF-SLUCM, 3 urban types can be distinguished: urban type 1 refers to low intensity residential urban (corresponding to the open space and low intensity developed land in NLCD), type 2 refers to the high intensity residential urban (corresponding to the medium intensity developed land in NLCD), and type 3 refers to the industrial and commercial urban (corresponding to the high intensity developed land in NLCD). Their distributions are shown in Figure 3d. The morphological and thermal properties associated with these three urban types are provided in Table S2 in Supporting Information S1. To achieve the above-mentioned correspondence between WRF-SLUCM and NLCD in terms of urban types, minor code modifications are required. Here it is noted that urban morphological and thermal properties are only a function of urban types and thus vary spatially in the same way as urban types. This assumption can be relaxed by supplying WRF-SLUCM with data sets of urban morphological and thermal properties that are independent of urban types. However, since our work does not focus much on the spatial variability of dT/dQ_{AH} within the domain, the effects of more detailed and higher-resolution urban morphological and thermal properties data on dT/dQ_{AH} are left for future studies.

We implement methods 2 and 3 of Q_{AH} release into SLUCM. We also implement the three SVs (Figures 1b–1d) into WRF-SLUCM. For SV 1, we conduct 4 different sets of simulations (no Q_{AH} and Q_{AH} released by method 1, method 2, and method 3, respectively). In the simulations with Q_{AH}, we use domain-uniform, time-invariant

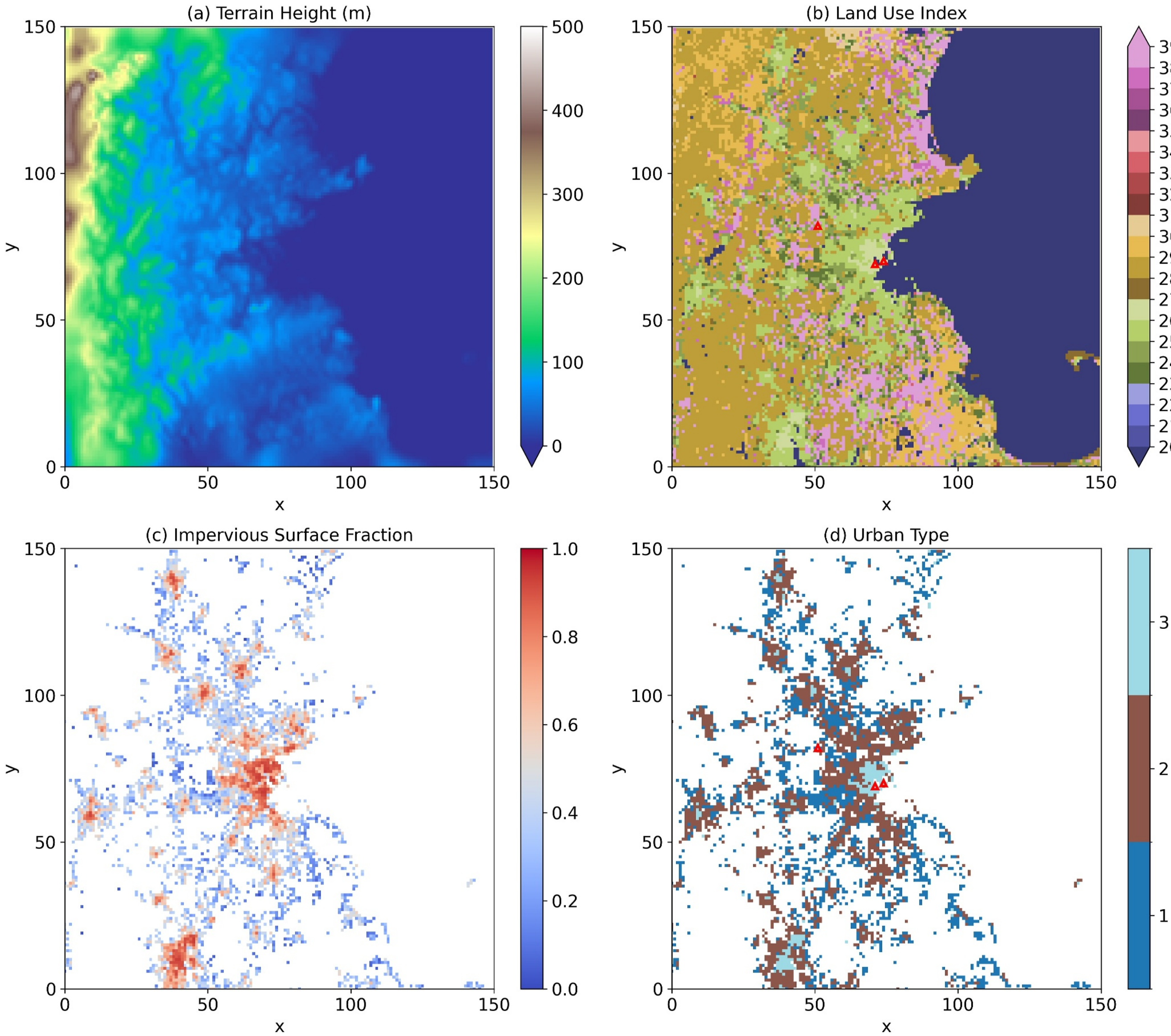

Figure 3. (a) Terrain height (m), (b) Land use index (see Table S1 in Supporting Information S1 for the classification scheme), (c) Impervious surface fraction, and (d) Urban type for the innermost domain where dx = dy = 1 km. The *x*-axis and *y*-axis refer to the number of grid cells in the west-east and south-north directions, respectively. The red triangles in (b) and (d) indicate the three weather stations where simulated and observed temperatures are compared.

values: 10 W m^{-2}, 50 W m^{-2}, and 100 W m^{-2}. Our choice of using domain-uniform, time-invariant Q_{AH} values is motivated by the fact that our focus is on the sensitivity of urban temperatures to Q_{AH} instead of simulating the real-world temperature responses (ΔT). For SVs 2 to 4, we conduct four sets of simulations (no Q_{AH}, and Q_{AH} handled by three methods with $Q_{AH} = 100$ W m^{-2}) for each SV. As will be seen later, we also revise method 1 and conduct 6 additional simulations with the revised method 1 (SV 1 with $Q_{AH} = 10$ W m^{-2}, 50 W m^{-2}, and 100 W m^{-2} and SVs 2–4 with $Q_{AH} = 100$ W m^{-2}). Table 1 provides a summary of the simulations conducted.

Here we should stress that the anthropogenic heat flux in WRF-SLUCM is defined as a flux *per unit area of impervious land*, not per unit area of grid cell. Hence, the anthropogenic heat flux defined as per unit area of grid cell is $Q_{AH} f_{urban}$. Given that f_{urban} varies spatially as shown in Figure 3c, the anthropogenic heat flux defined as per unit area of grid cell also varies spatially. The f_{urban} averaged over the innermost domain (including grid cells where $f_{urban} = 0$) is 0.077. Hence, the domain-averaged anthropogenic heat flux defined as per unit area of grid cell is $0.077 Q_{AH}$. So for $Q_{AH} = 100$ W m^{-2}, the domain-averaged anthropogenic heat flux is 7.7 W m^{-2}. In comparison,

Table 1
Summary of Weather Research and Forecasting Simulations

Structural variant	Q_{AH} release method	Q_{AH} value (W m^{-2})	Number of simulations
SV 1	No Q_{AH}	0	1
SV 1	Method 1	10, 50, 100	3
SV 1	Method 2	10, 50, 100	3
SV 1	Method 3	10, 50, 100	3
SV 1	Revised Method 1	10, 50, 100	3
SV 2 - 4	No Q_{AH}	0	3 (1 each)
SV 2 - 4	Method 1	100	3 (1 each)
SV 2 - 4	Method 2	100	3 (1 each)
SV 2 - 4	Method 3	100	3 (1 each)
SV 2 - 4	Revised Method 1	100	3 (1 each)

f_{urban} averaged over urban grid cells (where $f_{urban} > 0$) is 0.44. Hence, the urban-averaged anthropogenic heat flux defined as per unit area of grid cell is $0.44Q_{AH}$. So for $Q_{AH} = 100$ W m^{-2}, the urban-averaged anthropogenic heat flux is 44 W m^{-2}.

In addition to the Noah land surface model and SLUCM, other key physical parameterization schemes include: the WSM6 microphysical scheme (Hong, Lim, et al., 2006), the Dudhia shortwave radiation scheme (Dudhia, 1989), the Rapid Radiative Transfer Model longwave radiation scheme (Mlawer et al., 1997), the YSU boundary layer scheme (Hong, 2010; Hong, Noh, & Dudhia, 2006), and the revised MM5 surface layer scheme. Cumulus scheme is turned off for all domains because the largest grid size is less than 10 km (Stensrud, 2009).

To diagnose the contributions of various physical processes to dT/dQ_{AH}, certain variables that are not in the standard WRF outputs are needed. Of particular importance are the heat transfer resistances (r_R, r_W, r_G, r_C, r_U and r_2), which are parameterized (i.e., calculated internally) by WRF-SLUCM. The temperatures of various urban facets (T_R, T_W, T_G), the canopy air temperature (T_C), the grass surface temperature (T_{GRASS}), and the atmospheric temperature (T_A) are also outputted. All outputs are saved at hourly scales.

We simulate a 3-day heatwave period (20–22 July 2022) with boundary conditions from North American Regional Reanalysis (Mesinger et al., 2006). The simulations all start from 00 UTC of July 19 and end on 00 UTC of July 23, with July 19 treated as the spin-up. This event features westerly winds on July 20, transition to southerly winds on July 21, and then to westerly winds again on July 22. The near-surface wind speeds show diurnal variations. During the daytime, solar heating causes the boundary layer to grow, resulting in increased turbulent mixing. This mixing transports higher momentum air from aloft down to the surface, leading to stronger near-surface wind speeds. The domain-averaged 10 m wind speed simulated by WRF ranges from 2.2 m s^{-1} in the early morning of July 22 to 8 m s^{-1} in the late afternoon of July 21.

Figure 4 shows the comparison between the No Q_{AH} simulations and observations from three weather stations. The grid cells corresponding to these three weather stations are all classified as urban by WRF. From Figure 4, one can see that WRF does a reasonably good job in capturing the observed near-surface air temperature for all 4 SVs. The fact that simulated results from all 4 SVs agree reasonably well with observations suggest that they are all credible model SVs, which justifies our investigation of them.

Since the study by Wang et al. (2023) has examined the diurnal variability, our analysis will not tackle the diurnal variability but instead focus on the temporally averaged (over both day and night) results from 00UTC of July 20 to 00 UTC of July 23.

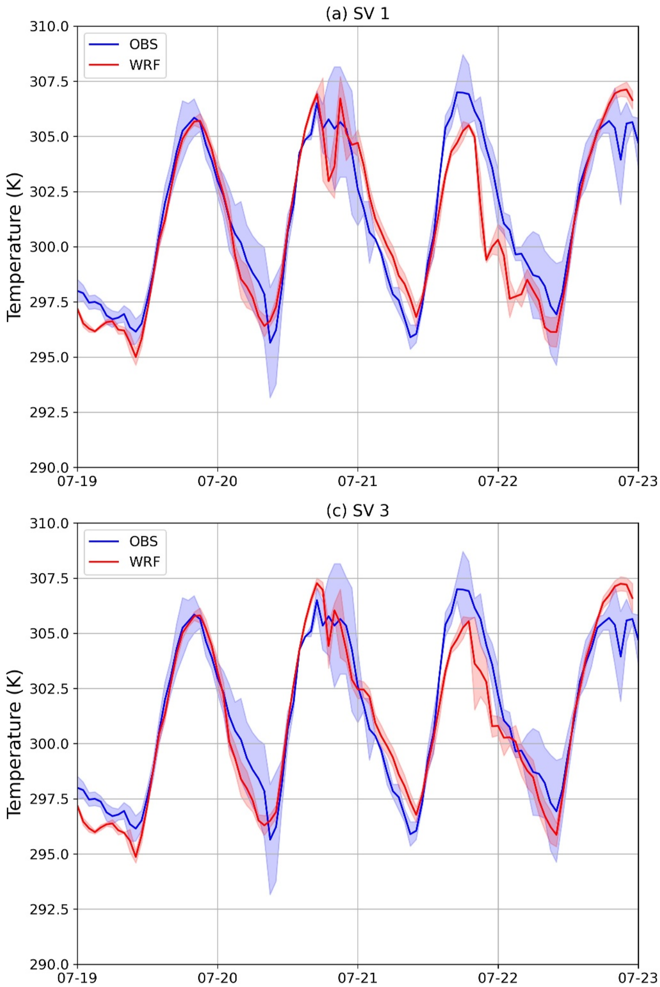

Figure 4. Comparison between simulated and observed near-surface air temperature at three urban stations whose locations are shown in Figure 3. The simulated temperatures are taken from the nearest grids from the stations. The four SVs correspond to the four panels in Figure 1. The simulations are with $Q_{AH} = 0$. Shading indicates the temperature range across the three stations.

3. Results

3.1. The Sensitivity of T_C to Q_{AH}

3.1.1. Q_{AH} Release Methods

Figures 5a–5c presents how dT_C/dQ_{AH} varies with the Q_{AH} release methods for simulations with $\Delta Q_{AH} = 10$ W m^{-2}. Figures 5d–5f further separates the results based on urban types. The spatial mean values of dT_C/dQ_{AH} range from 0.08 to 0.09 K/(W m^{-2}) for method 3, which are about 3–4 times those for method 1 (0.02–0.03 K/(W m^{-2})). The values for method 2 (0.05–0.06 K/(W m^{-2})) are 2–2.5 times those from method 1. The simulated dT_C/dQ_{AH} is much less dependent on urban types than on the Q_{AH} release methods, with the spatial mean values only slightly larger for urban type 3 (industrial and commercial urban land). Given the similarity of dT_C/dQ_{AH} across urban types, our following analysis of dT_C/dQ_{AH} will include all urban types. To understand these results, we decompose dT_C/dQ_{AH} into contributions from various factors using Equation 3, as follows

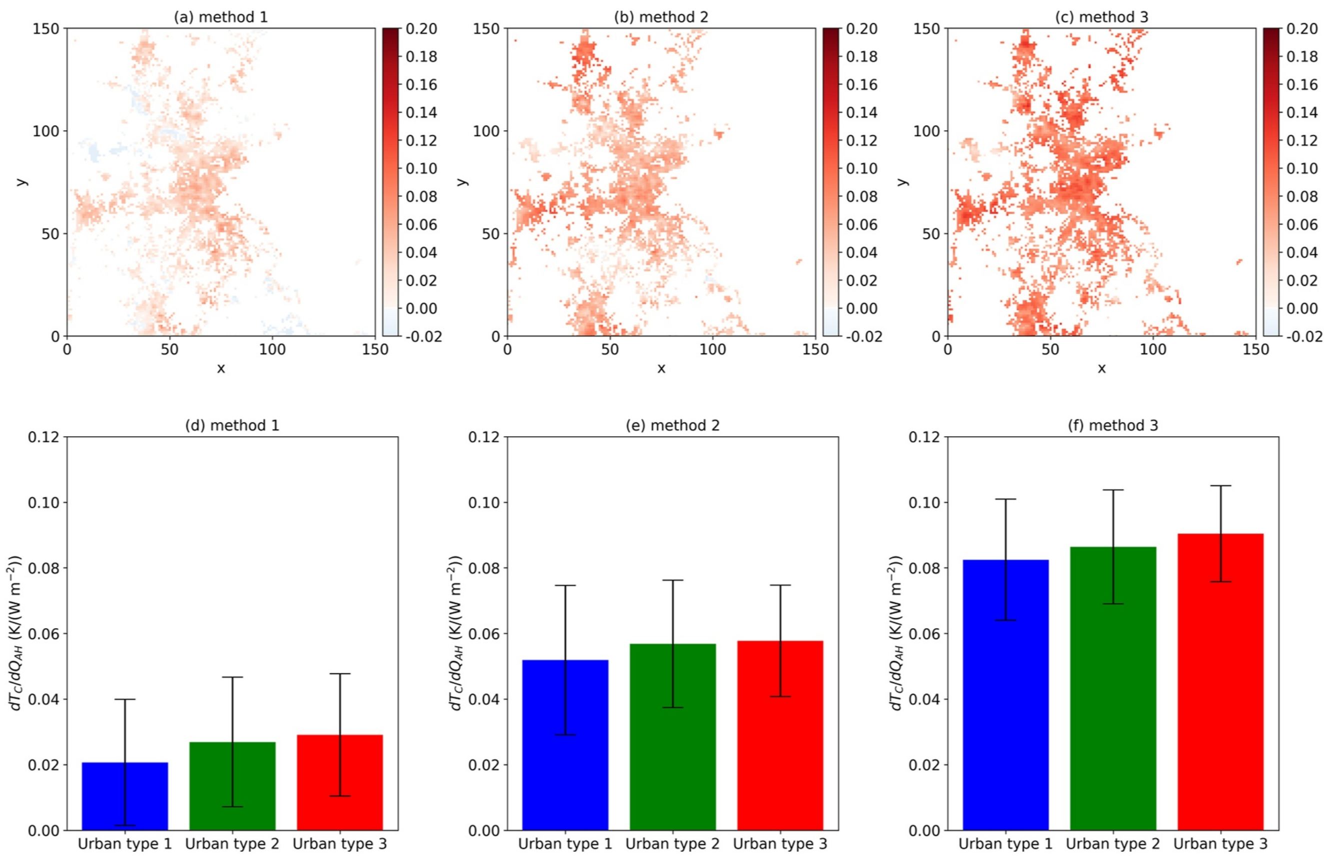

Figure 5. (a–c) Spatial patterns of dT_C/dQ_{AH} (unit: K/(W m^{-2})) across three Q_{AH} release methods in structural variants (SV) 1 (see Figure 1a and the associated texts for the differences among these three Q_{AH} release methods). (d–f) dT_C/dQ_{AH} (unit: K/(W m^{-2})) across three Q_{AH} release methods in SV 1 and across three different urban types. These results are for $\Delta Q_{AH} = 10$ W m^{-2}. The error bars are standard deviations across space and indicate spatial variability.

$$\begin{aligned}\frac{dT_C}{dQ_{AH}} = &\frac{\partial T_C}{\partial Q_{AH}} \\ &+\left(\frac{\partial T_C}{\partial r_W}\frac{dr_W}{dQ_{AH}}+\frac{\partial T_C}{\partial r_G}\frac{dr_G}{dQ_{AH}}\right) \\ &+\left(\frac{\partial T_C}{\partial T_W}\frac{dT_W}{dQ_{AH}}+\frac{\partial T_C}{\partial T_G}\frac{dT_G}{dQ_{AH}}\right) \\ &+\frac{\partial T_C}{\partial r_C}\frac{dr_C}{dQ_{AH}} \\ &+\frac{\partial T_C}{\partial T_A}\frac{dT_A}{dQ_{AH}}.\end{aligned} \tag{16}$$

The terms on the right-hand-side of Equation 16 refer to the baseline contribution, contribution from surface-canopy air resistances (r_W and r_G), contribution from surface temperatures (T_W and T_G), contribution from atmosphere-canopy air resistance (r_C), and contribution from atmospheric temperature (T_A) or atmospheric feedback. Each contribution is the product of the partial derivative and the total change. The partial derivatives can be analytically derived (see Supporting Information S1) and the total changes (represented by d, e.g., dr_C) are quantified as the difference between the results of the sensitivity simulations (with Q_{AH}) and those of the control simulation (no Q_{AH}). Another way of estimating the contribution of a particular parameter to the change in T_C is to keep all other parameters unchanged as in the control simulation, but replace the value of this particular parameter by its values in the sensitivity simulations in Equation 3 (e.g., Zhou et al., 2021).

Three important points should be stressed before we use the above decomposition method. First, this decomposition approach is not a unique way to decompose dT_C/dQ_{AH}. Here T_C is treated as a function of $Q_{AH}\delta_{i3}$, r_W,r_G,T_W,T_G,r_C, and T_A (see Equation 3), which are assumed to be independent variables. By treating T_C as a function of these variables (i.e., by employing Equation 3), the three Q_{AH} release methods will have different contribution patterns. Notably, there will be no baseline contribution in methods 1 and 2 because Q_{AH} can only affect T_C through T_A and T_G in method 1 and method 2, respectively. In theory, one could further express T_A and T_G as an explicit function of $Q_{AH}\delta_{i1}$ and $Q_{AH}\delta_{i2}$, respectively, as well as other variables. If so, there would be baseline contributions in methods 1 and 2. However, we choose not to do so since the relation between T_A (T_G) and $Q_{AH}\delta_{i1}$ ($Q_{AH}\delta_{i2}$) is complicated and not always analytical. Second, this decomposition approach appears different from the forcing-feedback framework introduced by Wang et al. (2023) in that the quantity analyzed here is the total sensitivity while the forcing-feedback framework analyzes the total feedback parameter, which is the negative reciprocal of the total sensitivity. The two approaches should yield similar qualitative understanding though. Third, before examining the decomposition results, a comparison between WRF outputted T_C and diagnosed T_C using Equation 3 should be conducted, as shown in Figure S1 in Supporting Information S1. One can see that the diagnosed T_C matches the WRF outputted T_C exactly, which gives us confidence in using Equation 3 and thus Equation 16 to decompose dT_C/dQ_{AH} into various contributions.

Figure 6 shows the decomposition results of dT_C/dQ_{AH} with $\Delta Q_{AH} = 10$ W m^{-2} (a-c), $\Delta Q_{AH} = 50$ W m^{-2} (d-f), $\Delta Q_{AH} = 100$ W m^{-2} (g-i). A few interesting features are worth pointing out. First, across all panels the summed contribution from all factors (the second bar) matches the directly computed $dT_C/dQ_{AH} = \Delta T_C/\Delta Q_{AH}$ (the first bar), suggesting the robustness of the decomposition method. This is consistent with the results shown in Figure S1 in Supporting Information S1. Second, only method 3 (panels c, f, and i) has baseline contributions while the other two methods do not, as Q_{AH} only explicitly appears in the canopy air energy budget in method 3. Third, contributions from surface-canopy air resistances and atmosphere-canopy air resistance are relatively small, at least when compared to the other contributions. Therefore, it can be concluded that dT_C/dQ_{AH} is mainly influenced by the baseline contributions, contributions from surface temperatures, as well as contributions from the atmospheric temperature (i.e., atmospheric feedback). The atmospheric feedback is particularly important for method 1.

It is clear that the most important contribution for method 2 is that from surface temperatures (including the canyon ground surface temperature T_G) while the other contributions are nearly negligible. This is not too surprising given that the Q_{AH} is added to the canyon ground surface energy budget in method 2. In comparison, one might expect the atmospheric temperature contribution and the baseline contribution to be dominant in method 1 and method 3, respectively, given that Q_{AH} is added to the atmospheric temperature budget equation in method 1 and the canopy air temperature budget equation in method 3. However, the contributions from surface temperatures are not negligible in those two methods. In fact, they are as important as the atmospheric temperature contribution and the baseline contribution.

The results are quite consistent for different ΔQ_{AH} values, especially for methods 2 and 3, suggesting limited nonlinearity in the response of T_C to increasing Q_{AH}. Even for method 1, the results are not inconsistent across different ΔQ_{AH} values given the large error bars in the scenario of $\Delta Q_{AH} = 10$ W m^{-2}. The error bars here indicate the spatial variability. The gradual reduction of error bars as ΔQ_{AH} increases suggests that dT_C/dQ_{AH} tends to converge as the magnitude of Q_{AH} increases. This demonstrates that the behavior of the temperature sensitivity (dT_C/dQ_{AH}) is more constrained than that of the temperature response ΔT_C, which makes it a better quantity to measure the effect of anthropogenic heat flux. Using the seemingly converged values for dT_C/dQ_{AH} in simulations with $\Delta Q_{AH} = 100$ W m^{-2}, we can see that dT_C/dQ_{AH} can differ by an order of magnitude between method 1 (0.007 K/(W m^{-2})) and method 3 (0.08 K/(W m^{-2})) (see Table 2).

The study by Wang et al. (2023) also used method 3 and a comparison between our results and theirs is warranted, noting though the differences in terms of model structures (CLMU vs. WRF-SLUCM), spatial/temporal spans of model simulations, and offline versus land-atmosphere coupled simulations. The negligible contribution from surface-canopy air resistances (r_W and r_G) is consistent with their finding. However, the magnitude of the baseline contribution here is much larger than that in Wang et al. (2023). Moreover, Wang et al. (2023) reported that the positive contribution from surface temperatures is nearly canceled by the negative contribution from r_C in summer, which is different from our finding that the negative contribution from r_C is much smaller (in magnitude) than the positive contribution from surface temperatures (see panels c, f, and i). As shall be seen later, these

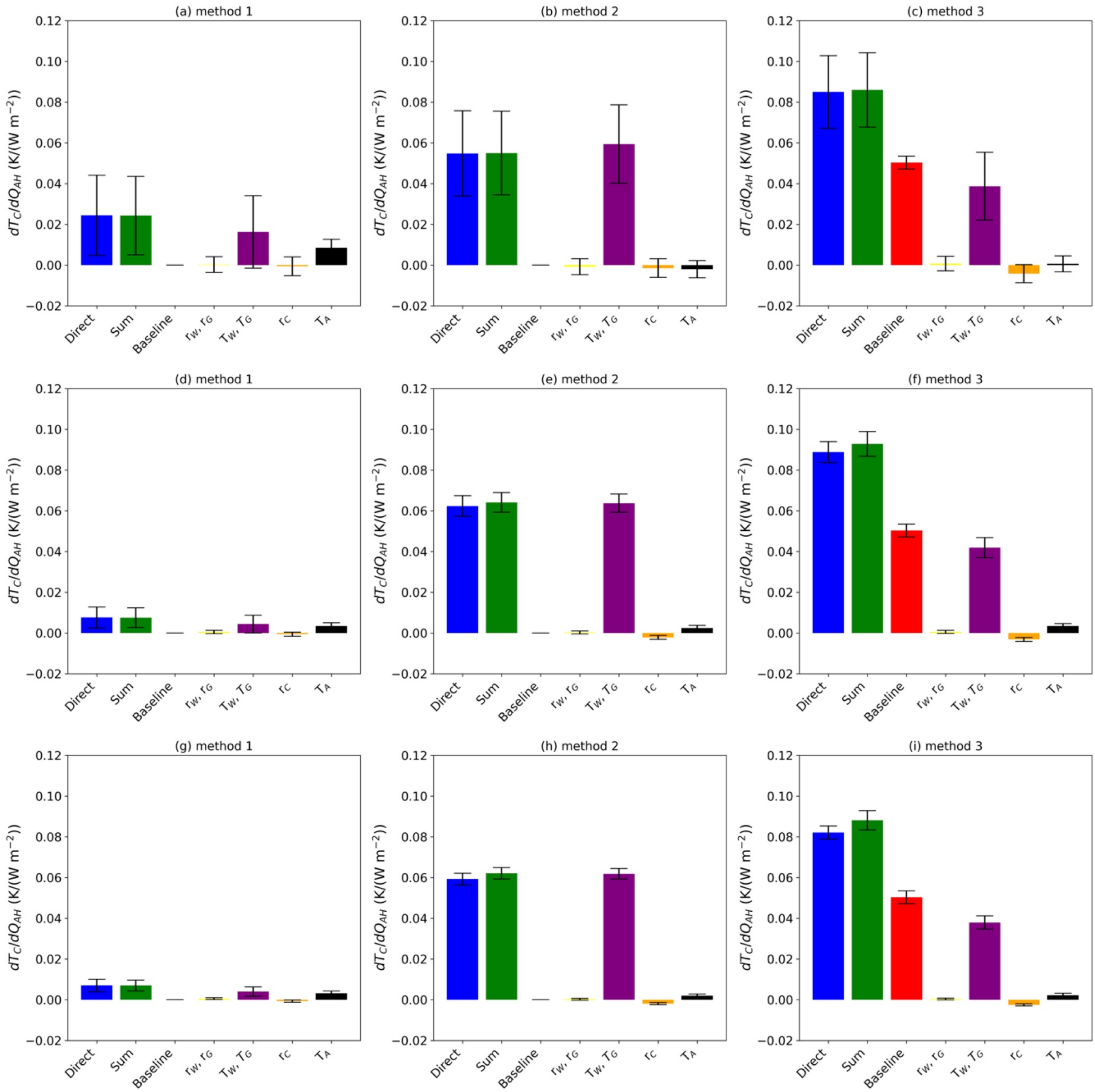

Figure 6. Decomposition of dT_C/dQ_{AH} (unit: K/(W m^{-2})) estimated with three Q_{AH} release methods for (a–c) $\Delta Q_{AH} = 10$ W m^{-2}, (d–f) $\Delta Q_{AH} = 50$ W m^{-2}, (g–i) $\Delta Q_{AH} = 100$ W m^{-2}. The error bars are standard deviations across space and indicate spatial variability.

differences are partly related to the differences between the two models (CLMU and WRF-SLUCM) in terms of the treatment of roof-air interaction and the parameterization of r_C.

3.1.2. Structural Variants of SLUCM

Figure 7 shows the decomposition results of dT_C/dQ_{AH} for the 4 SVs (i.e., the four panels in Figure 1) with method 3 and $Q_{AH} = 100$ W m^{-2}. The results for SV 1 are identical to Figure 6i but are reproduced enabling a direct comparison. Note that for SVs 2 and 4, the decomposition is performed using Equation 5 following

Table 2
Summary of dT/dQ_{AH} (Unit: K/(W m^{-2})) Values

	Methods	SV 1	SV 2	SV 3	SV 4
dT_C/dQ_{AH}	Method 1	0.007	0.003	0.009	0.007
	Method 2	0.06	0.03	0.02	0.015
	Method 3	0.08	0.045	0.03	0.02
dT_S/dQ_{AH}	Revised Method 1	0.005	0.004	0.006	0.005
	Method 2	0.017	0.014	0.021	0.021
	Method 3	0.022	0.022	0.028	0.027
dT_2/dQ_{AH}	Revised Method 1	0.006	0.005	0.007	0.007
	Method 2	0.008	0.005	0.01	0.01
	Method 3	0.01	0.009	0.013	0.012

Note. These values are averaged over all urban types and for $\Delta Q_{AH} = 100$ W m^{-2}.

$$\frac{dT_C}{dQ_{AH}} = \frac{\partial T_C}{\partial Q_{AH}} + \left(\frac{\partial T_C}{\partial r_R}\frac{dr_R}{dQ_{AH}} + \frac{\partial T_C}{\partial r_W}\frac{dr_W}{dQ_{AH}} + \frac{\partial T_C}{\partial r_G}\frac{dr_G}{dQ_{AH}}\right) + \left(\frac{\partial T_C}{\partial T_R}\frac{dT_R}{dQ_{AH}} + \frac{\partial T_C}{\partial T_W}\frac{dT_W}{dQ_{AH}} + \frac{\partial T_C}{\partial T_G}\frac{dT_G}{dQ_{AH}}\right) + \frac{\partial T_C}{\partial r_C}\frac{dr_C}{dQ_{AH}} + \frac{\partial T_C}{\partial T_A}\frac{dT_A}{dQ_{AH}} \tag{17}$$

where the roof temperature (T_R) and roof-canopy air resistance (r_R) are included.

Comparing SV 2 to SV 1 reveals that the baseline contribution is reduced in SV 2. This is because $\partial T_C/\partial Q_{AH}$ is always smaller in SV 2 than in SV 1. From Equation 3 for SV 1, we can derive

$$\frac{\partial T_C}{\partial Q_{AH}} = \frac{(R+G)\frac{1}{C_a}\delta_{3i}}{\frac{2H}{r_W} + \frac{G}{r_G} + \frac{G}{r_C}} = \frac{1}{\frac{2H}{R+G}\frac{1}{r_W} + \frac{G}{R+G}\frac{1}{r_G} + \frac{G}{R+G}\frac{1}{r_C}}\left(\frac{1}{C_a}\delta_{3i}\right). \tag{18}$$

Similarly, Equation 5 for SV 2 gives

$$\frac{\partial T_C}{\partial Q_{AH}} = \frac{(R+G)\frac{1}{C_a}\delta_{3i}}{\frac{R}{r_R} + \frac{2H}{r_W} + \frac{G}{r_G} + \frac{R+G}{r_C}} = \frac{1}{\frac{R}{R+G}\frac{1}{r_R} + \frac{2H}{R+G}\frac{1}{r_W} + \frac{G}{R+G}\frac{1}{r_G} + \frac{1}{r_C}}\left(\frac{1}{C_a}\delta_{3i}\right). \tag{19}$$

Comparing Equation 19 to Equation 18 indicates that $\partial T_C/\partial Q_{AH}$ always becomes smaller in SV 2 than in SV 1. Physically this reduction is because Q_{AH} is distributed over a larger area in SV 2 than in SV 1. In SV 1, by separating the roof from the canyon, the canopy air effectively only exists over the canyon; while in SV 2, the canopy air exists over both roof and canyon.

One can also show that $\partial T_C/\partial T_W$ and $\partial T_C/\partial T_G$ are smaller in SV 2 than in SV 1 (see Supporting Information S1). Although the roof surface provides an additional feedback pathway, its contribution does not overcome the reduced contributions from T_W and T_G. This explains why the contribution from all surface temperatures (T_R, T_W, and T_G) is smaller in SV 2 than in SV 1. It can be further shown that $\partial T_C/\partial T_A$ (see Supporting Information S1) is larger in SV 2 than in SV 1, which is consistent with that the contribution of T_A is slightly higher in SV 2 than in SV 1.

Figure 7c shows that when r_C is computed with the momentum roughness length (SV 3), the baseline contribution is reduced. This can be inferred from Equation 18, which shows that $\partial T_C/\partial Q_{AH}$ decreases with decreasing r_C. It can be also shown $\partial T_C/\partial T_W$ and $\partial T_C/\partial T_G$ (see Supporting Information S1) are reduced with decreasing r_C, thereby explaining the reduced contribution from surface temperatures. In contrary, $\partial T_C/\partial T_A$ increases with decreasing r_C. Physically it means that as convective heat transfer between the canopy air and the atmosphere becomes stronger, the canopy air temperature is more strongly affected by the atmospheric temperature. Together with a larger ΔT_A as a result of a stronger Q_C in SV 3, the contribution of T_A is increased in SV 3 than in SV 1.

The combined effect of changing the treatment of roof-air interaction and the parameterization of r_C toward CLMU-like (i.e., comparing SV 4 to SV 1 or comparing Figure 7d to Figure 7a) is that the total sensitivity value changes by a factor of 4 (from about 0.08 to 0.02 K/(W m^{-2})) and agrees better with those presented in Wang et al. (2023). The baseline sensitivity in SV 4 is about 0.014 K/(W m^{-2}), which is in much better agreement with the values in Wang et al. (2023). The positive contribution from surface temperatures in SV 4 becomes closer to the negative contribution from r_C, which is also in better agreement with that in Wang et al. (2023), even though they do not cancel each other. The contribution of atmospheric feedback is slightly positive (0.006 K/(W m^{-2})).

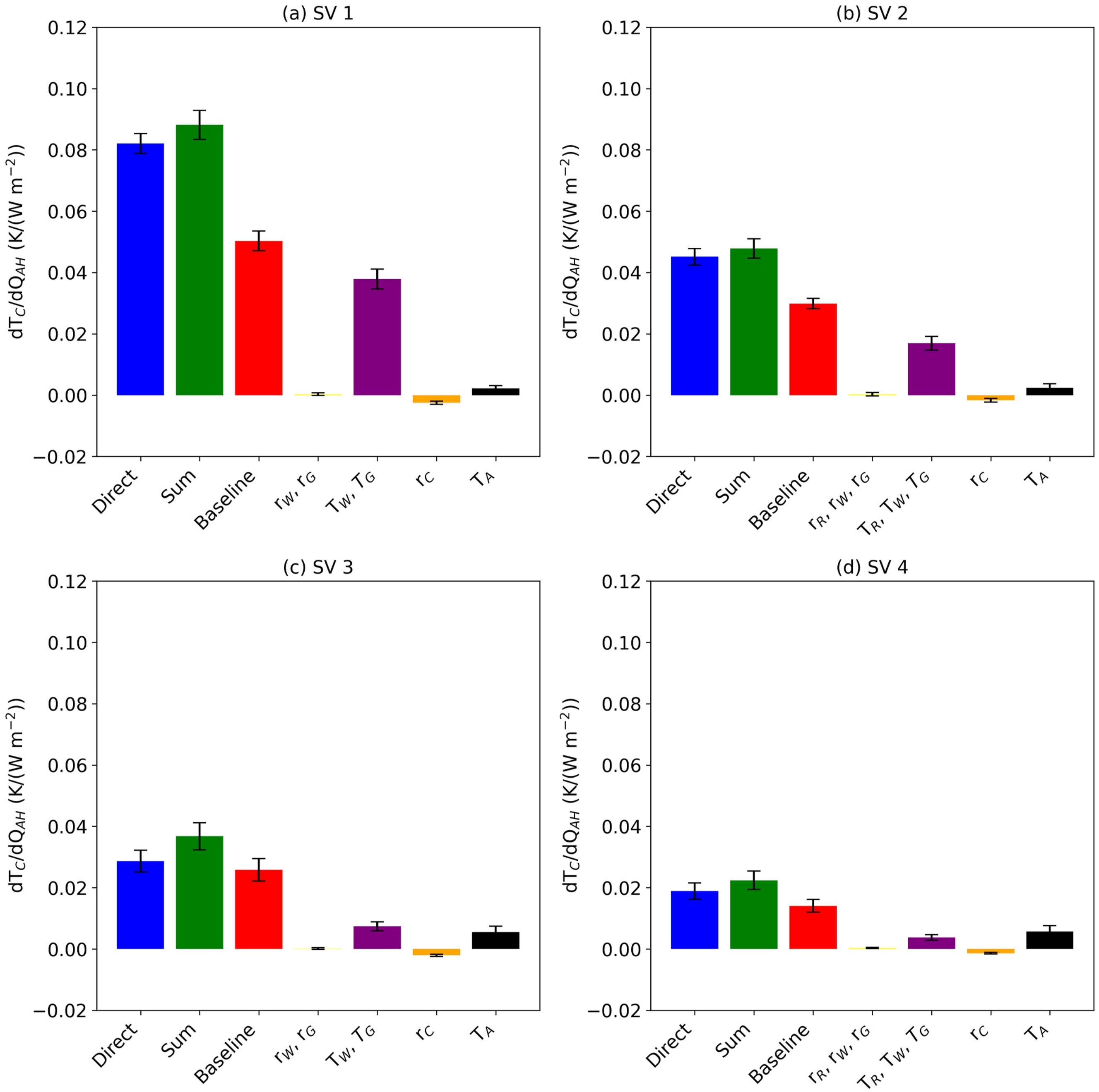

Figure 7. Decomposition of dT_C/dQ_{AH} (unit: K/(W m^{-2})) estimated with method 3 but for four different SVs (see Figure 1). These results are for $\Delta Q_{AH} = 100$ W m^{-2}. The error bars are standard deviations across space and indicate spatial variability.

The much better agreement between our SV 4 results and those in Wang et al. (2023) implies that the treatment of roof-air interaction and the parameterization of r_C could be the main cause of the differences between our SV 1 results and theirs.

The results from SV 4 demonstrate that atmospheric feedback (i.e., contribution from T_A) needs to be considered for such a configuration. In this configuration, the canopy air is implicitly distributed over the entire impervious land (roof and canyon) instead of just over the canyon and the connection between the canopy air and the atmosphere is stronger due to a smaller heat transfer resistance, both effects promoting the importance of atmospheric feedback in controlling the dynamics of T_C.

3.2. The Sensitivities of T_S and T_2 to Q_{AH}

The first part of this study focuses solely on canopy air temperature (T_C). In the second part, we turn our attention to two other temperature variables, surface temperature (T_S) and 2-m air temperature (T_2). Unlike T_C that is a prognostic temperature variable, both T_S and T_2 are diagnostic temperatures in the land surface model (although as shall be seen later T_S is a prognostic temperature if one considers the atmospheric model).

3.2.1. Q_{AH} Release Methods: A Revised Method 1

Figure S2 in Supporting Information S1 shows a comparison between dT_C/dQ_{AH} (first row), dT_S/dQ_{AH} (second row), and dT_2/dQ_{AH} (third row) across three Q_{AH} release methods, with $\Delta Q_{AH} = 100$ W m^{-2} and SV 1. It is surprising that dT_S/dQ_{AH} (and dT_2/dQ_{AH}) is the strongest in method 1, which is inconsistent with that dT_C/dQ_{AH} is the weakest in method 1. To explain this surprising result, we further examine the sensitivities of all prognostic surface temperatures, including T_R, T_W, T_G, and T_{GRASS}, as shown in Figure S3 in Supporting Information S1. By comparing these results in method 1 and those in methods 2 and 3, it is difficult to understand why dT_S/dQ_{AH} is the strongest in method 1, as all these prognostic surface temperatures show either very similar (T_R and T_{GRASS}) or much smaller (T_W and T_G) sensitivities to Q_{AH} in method 1 compared to methods 2 and 3.

The cause for this peculiar result is one key assumption in method 1. In method 1, Q_{AH} is supposedly added to the heat budget of the atmosphere. However, to simplify the coding, Q_{AH} is added to Q_U in method 1, resulting in

$$Q_U = Q_R \frac{R}{R+G} + Q_W \frac{2H}{R+G} + Q_G \frac{G}{R+G} + Q_{AH}\delta_{3i} + Q_{AH}\delta_{1i}. \tag{20}$$

Here the term with δ_{3i} is due to energy balance while the term with δ_{1i} is an assumption. While this assumption might be acceptable from the perspective of atmospheric modeling (i.e., the sum of sensible heat flux and Q_{AH} is the total heating source for the atmosphere), adding Q_{AH} to the sensible heat flux will *instantaneously* increase T_S and T_2 through Equations 12 and 15. The more physically based approach is to add Q_{AH} into the heat budget of the atmosphere instead of combining it with the sensible heat flux. One can imagine that if Q_{AH} was added to the heat budget of the atmosphere while the sensible heat flux (Q_U) was computed with Equation 10, T_S and T_2 would not *instantaneously* increase with Q_{AH}. Under such conditions, Q_{AH} affects T_S and T_2 by warming the atmosphere first.

We implement such a change in WRF-SLUCM for method 1 where Q_{AH} does not directly show up in the calculation of T_S and T_2. In other words, Q_U is computed with Equation 10 instead of Equation 20. The results with the revised method 1 are shown in Figures S4 and S5 in Supporting Information S1. If T_S and T_2 were purely diagnostic variables, the method 1 and revised method 1 should give identical prognostic results. However, the minor changes in the T_C results (cf. Figure S4 to Figure S2 in Supporting Information S1), as well as minor changes in the prognostic surface temperatures (cf. Figure S5 to Figure S3 in Supporting Information S1), suggest that this is not the case. This is because while T_S is not used in any prognostic calculations in the land surface model, it is used by the radiation schemes of the atmospheric model to estimate the upward longwave radiation, which renders it a (semi-)prognostic variable. Hence, when T_S changes between method 1 and revised method 1, the prognostic results (e.g., T_C) are altered. However, changes in prognostic results are quite small (cf. Figure S5 to Figure S3 in Supporting Information S1).

The more significant changes between method 1 and revised method 1 are associated with T_S and T_2, as expected. Comparing Figure S4 to Figure S2 in Supporting Information S1, dT_S/dQ_{AH} and dT_2/dQ_{AH} are greatly reduced in the revised method 1 than in the method 1. Moreover, the rankings of dT_S/dQ_{AH} and dT_2/dQ_{AH} across the 3 methods (Figure S4 in Supporting Information S1) are in better agreement with those for the prognostic temperatures (Figures S4 and S5 in Supporting Information S1). These results suggest that the T_S and T_2 in the revised method 1 are more consistent with prognostic temperature variables than those in the method 1.

3.2.2. Q_{AH} Release Methods: T_S

With the revised method 1, Figure 8 compares how dT_S/dQ_{AH} from the revised method 1 differs from that in the other two Q_{AH} release methods for simulations with $\Delta Q_{AH} = 100$ W m^{-2}. The spatial mean values of dT_S/dQ_{AH} are 0.004–0.008 K/(W m^{-2}) for revised method 1. The spatial mean values of dT_S/dQ_{AH} for method 3

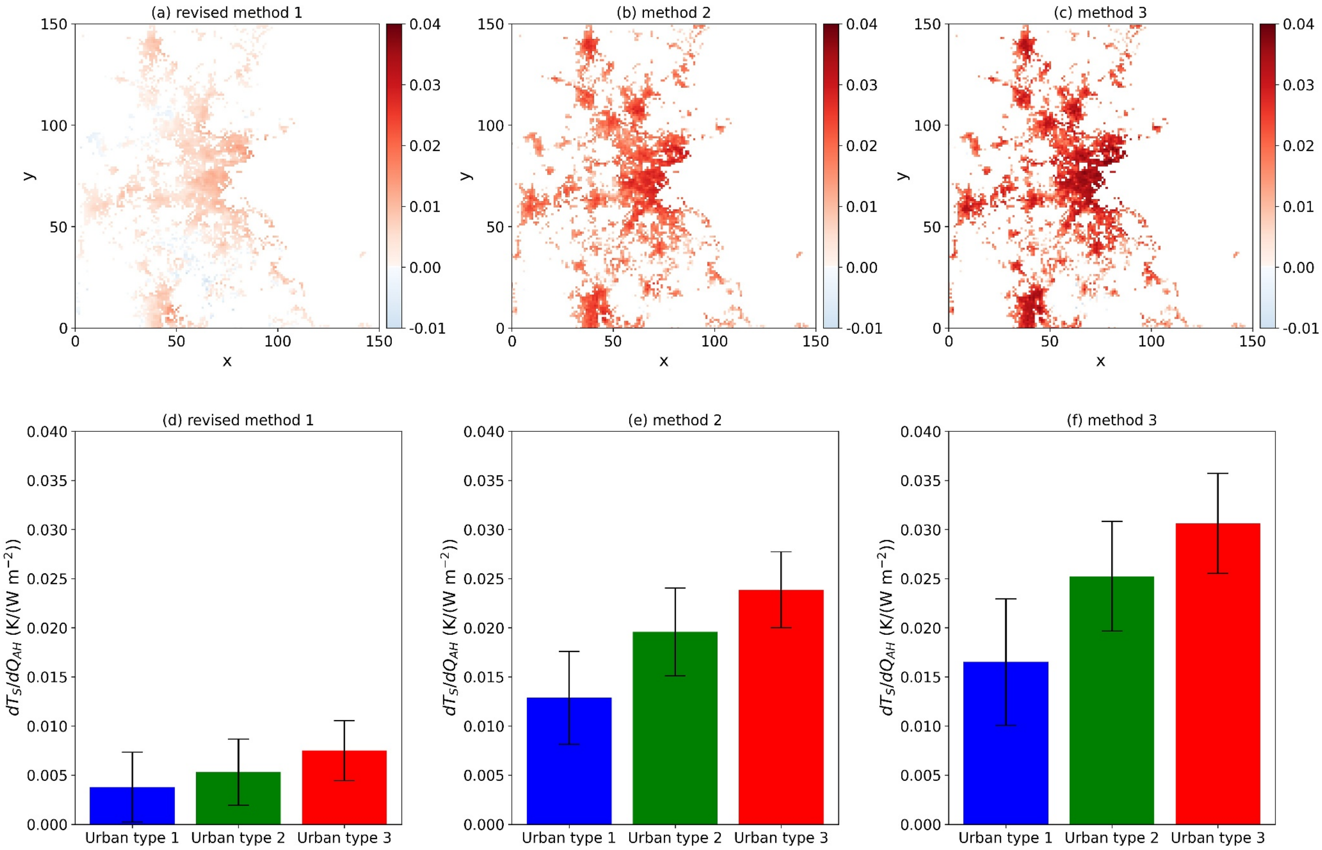

Figure 8. (a–c) Spatial patterns of dT_S/dQ_{AH} (unit: K/(W m^{-2})) across three Q_{AH} release methods. (d–f) dT_S/dQ_{AH} (unit: K/(W m^{-2})) across three Q_{AH} release methods and across three different urban types. These results are for $\Delta Q_{AH} = 100$ W m^{-2}.

(0.017–0.033 K/(W m^{-2})) are about 4 times those for revised method 1, while the values for method 2 (0.012–0.020 K/(W m^{-2})) are 2.5–3 times those for revised method 1. Compared to the results for dT_C/dQ_{AH}, dT_S/dQ_{AH} shows a stronger dependence on urban types than dT_C/dQ_{AH} (cf., Figures 5 and 8).

To explain the stronger urban type dependence of dT_S/dQ_{AH} and also to understand the processes controlling dT_S/dQ_{AH}, we decompose dT_S/dQ_{AH} into contributions from various factors. To do so, we need to utilize Equations 3, 10 and 12. Moreover, we need to utilize the definitions of Q_R, Q_W, and Q_G (below Equation 2). With all these equations, T_S becomes a function of prognostic temperature variables (i.e., T_R, T_W, T_G, T_{GRASS}, T_A), resistances (i.e., r_R, r_W, r_G, r_C, r_U), and $Q_{AH}\delta_{i3}$. Hence, the decomposition follows:

$$\begin{aligned}\frac{dT_S}{dQ_{AH}} = & \frac{\partial T_S}{\partial Q_{AH}} \\ & + \left(\frac{\partial T_S}{\partial r_R}\frac{dr_R}{dQ_{AH}} + \frac{\partial T_S}{\partial r_W}\frac{dr_W}{dQ_{AH}} + \frac{\partial T_S}{\partial r_G}\frac{dr_G}{dQ_{AH}} + \frac{\partial T_S}{\partial r_C}\frac{dr_C}{dQ_{AH}} + + \frac{\partial T_S}{\partial r_U}\frac{dr_U}{dQ_{AH}}\right) \\ & + \left(\frac{\partial T_S}{\partial T_R}\frac{dT_R}{dQ_{AH}} + \frac{\partial T_S}{\partial T_W}\frac{dT_W}{dQ_{AH}} + \frac{\partial T_S}{\partial T_G}\frac{dT_G}{dQ_{AH}} + \frac{\partial T_S}{\partial T_{GRASS}}\frac{dT_{GRASS}}{dQ_{AH}}\right) \\ & + \frac{\partial T_S}{\partial T_A}\frac{dT_A}{dQ_{AH}}.\end{aligned} \tag{21}$$

Note that we do not include T_C in the decomposition because it can be expressed as a function of other temperature variables through Equation 3. The terms on the right-hand-side of Equation 21 are organized as the baseline contribution, contribution from resistances, contribution from surface temperatures, and contribution from atmospheric temperature.

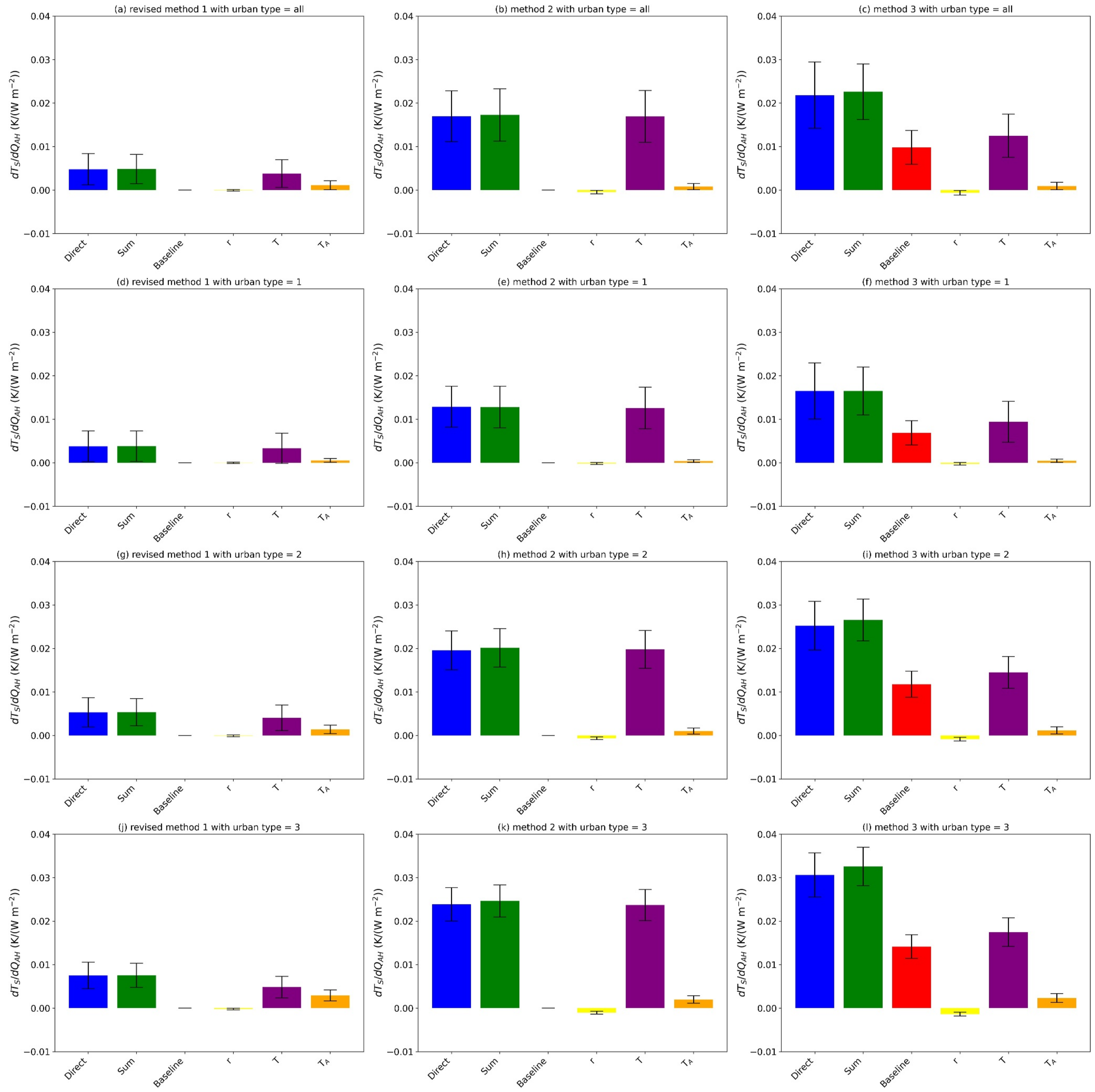

Figure 9. Decomposition of dT_S/dQ_{AH} (unit: K/(W m^{-2})) estimated with three Q_{AH} release methods for $\Delta Q_{AH} = 100$ W m^{-2}. From top to bottom: all urban types, urban type 1, urban type 2, urban type 3.

Again we should acknowledge that by treating T_S as a function of T_A and T_G (as well as other variables), only method 3 will have baseline contribution. For the revised method 1 and method 2, the influence of Q_{AH} on T_S is communicated through T_A and T_G, respectively. Note that the default method 1 would also include baseline contributions due to the treatment of Q_{AH} in method 1 (see Equation 20). The revised method 1, on the other hand, removes the baseline contributions for dT_S/dQ_{AH}, as elaborated in the previous section.

A comparison between WRF outputted T_S and our diagnosed T_S is conducted. As shown in Figure S6 in Supporting Information S1, the diagnosed T_S matches the WRF outputted T_S exactly. Figure 9 shows the decomposition results of dT_S/dQ_{AH} with $\Delta Q_{AH} = 100$ W m^{-2}. The decomposition is performed for all urban grid cells (a-c), urban type 1 (d-f), urban type 2 (g-i), and urban type 3 (j-l). Across the three methods, contributions from resistances are relatively small, making dT_S/dQ_{AH} mainly influenced by baseline contributions, contributions from surface temperatures, and contributions from atmospheric temperature. Among the surface temperatures, those making important contributions are the canyon ground temperature and wall temperature, as can be inferred from Figure S5 in Supporting Information S1.

Both baseline contributions and surface temperature contributions show a much stronger dependence on urban types than their counterparts for dT_C/dQ_{AH}. For baseline contributions, this can be inferred from $\partial T_S/\partial Q_{AH}$. For SVs 1 and 3, one can show

$$\frac{\partial T_S}{\partial Q_{AH}} = f_{urban} r_U \left(\frac{\frac{G}{R+G}\frac{1}{r_C}}{\frac{2H}{R+G}\frac{1}{r_W} + \frac{G}{R+G}\frac{1}{r_G} + \frac{G}{R+G}\frac{1}{r_C}} \right) \left(\frac{1}{C_a}\delta_{3i} \right). \tag{22}$$

For SVs 2 and 4, one can show

$$\frac{\partial T_S}{\partial Q_{AH}} = f_{urban} r_U \left(\frac{\frac{1}{r_C}}{\frac{2H}{R+G}\frac{1}{r_W} + \frac{1}{r_G} + \frac{1}{r_C}} \right) \left(\frac{1}{C_a}\delta_{3i} \right). \tag{23}$$

The impervious surface fraction f_{urban} explicitly shows up in $\partial T_S/\partial Q_{AH}$ (see both Equations 22 and 23), which is in contrast to the results for $\partial T_C/\partial Q_{AH}$ (see Equations 18 and 19). One can also show that the partial derivatives of T_S with respect to surface temperatures like T_W and T_G are also strongly and positively dependent on f_{urban} (see Supporting Information S1), which is why the surface temperature contributions are dependent on urban types. Although the atmospheric temperature contributions are small, the partial derivative of T_S with respect to atmospheric temperature $(\partial T_S/\partial T_A)$ also depends on f_{urban} (see Supporting Information S1) and thus atmospheric temperature contributions show dependence on urban types. As a result, dT_S/dQ_{AH} shows an overall dependence on urban types.

A more intuitive way to understand the urban type dependence of dT_S/dQ_{AH} is to recognize that Q_{AH} is defined as a flux per unit area of *impervious* land while T_S is a temperature for the entire *grid cell*. With the same amount of Q_{AH} per unit area of *impervious* land, grid cells with higher fractions of impervious land receive stronger heat inputs per unit area of *grid cell*. This is why grid cells of urban type 3 (industrial and commercial urban land), which have higher impervious surface fractions, tend to have higher values of dT_S/dQ_{AH}.

3.2.3. Q_{AH} Release Methods: T_2

Figure 10 compares dT_2/dQ_{AH} across three Q_{AH} release methods for simulations with $\Delta Q_{AH} = 100$ W m^{-2}. As can be seen, dT_2/dQ_{AH} differ less across the three methods than dT_C/dQ_{AH} and dT_S/dQ_{AH}. The spatial mean values of dT_2/dQ_{AH} are 0.004–0.009 K/(W m^{-2}) for the revised method 1, 0.007–0.01 K/(W m^{-2}) for method 2, and 0.008–0.012 K/(W m^{-2}) for method 3. Namely, the values for method 3 are about 1.5–2 times the values in the revised method 1. In terms of spatial variability, dT_2/dQ_{AH} shows some dependence on urban types, which is stronger than dT_C/dQ_{AH} but weaker than dT_S/dQ_{AH}.

Similar to the decomposition for dT_S/dQ_{AH}, we decompose dT_2/dQ_{AH} by utilizing Equations 3, 10, 12 and 15, and definitions of Q_R, Q_W, and Q_G. With these equations, T_2 becomes a function of prognostic temperature variables (i.e., T_R, T_W, T_G, T_{GRASS}, T_A), resistances (i.e., r_R, r_W, r_G, r_C, r_U, r_2), and $Q_{AH}\delta_{i3}$. The T_2 diagnosed this way matches the WRF outputted T_2 exactly as shown in Figure S7 in Supporting Information S1. Based on this, we can decompose dT_2/dQ_{AH} following

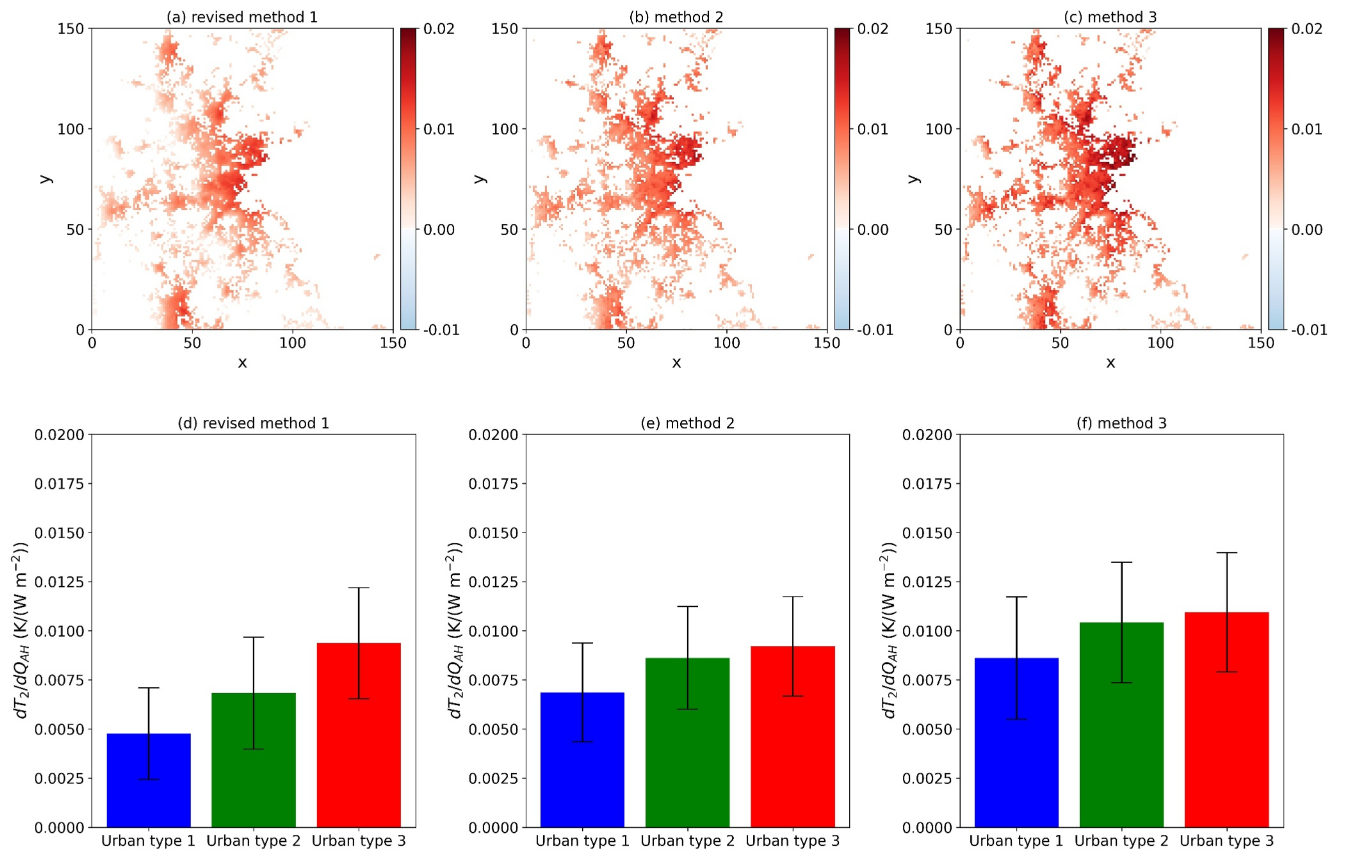

Figure 10. (a–c) Spatial patterns of dT_2/dQ_{AH} (unit: K/(W m^{-2})) across three different Q_{AH} release methods. (d, e, f) dT_2/dQ_{AH} (unit: K/(W m^{-2})) across three Q_{AH} release methods and across three different urban types. These results are for $\Delta Q_{AH} = 100$ W m^{-2}.

$$\begin{aligned}\frac{dT_2}{dQ_{AH}} = & \frac{\partial T_2}{\partial Q_{AH}} \\ & + \left(\frac{\partial T_2}{\partial r_R}\frac{dr_R}{dQ_{AH}} + \frac{\partial T_2}{\partial r_W}\frac{dr_W}{dQ_{AH}} + \frac{\partial T_2}{\partial r_G}\frac{dr_G}{dQ_{AH}} + \frac{\partial T_2}{\partial r_C}\frac{dr_C}{dQ_{AH}} + \frac{\partial T_2}{\partial r_U}\frac{dr_U}{dQ_{AH}} + \frac{\partial T_2}{\partial r_2}\frac{dr_2}{dQ_{AH}}\right) \\ & + \left(\frac{\partial T_2}{\partial T_R}\frac{dT_R}{dQ_{AH}} + \frac{\partial T_2}{\partial T_W}\frac{dT_W}{dQ_{AH}} + \frac{\partial T_2}{\partial T_G}\frac{dT_G}{dQ_{AH}} + \frac{\partial T_2}{\partial T_{GRASS}}\frac{dT_{GRASS}}{dQ_{AH}}\right) \\ & + \frac{\partial T_2}{\partial T_A}\frac{dT_A}{dQ_{AH}}.\end{aligned} \tag{24}$$

The terms on the right-hand-side of Equation 24 are the baseline contribution, contribution from resistances, contribution from surface temperatures, and contribution from atmospheric temperature.

Figure 11 shows the decomposition results of dT_2/dQ_{AH} with $\Delta Q_{AH} = 100$ W m^{-2}. Across the three methods, the main contributions for dT_2/dQ_{AH} are contributions from surface temperatures (especially canyon ground and wall temperatures), contributions from atmospheric temperature, and the baseline contributions (only for method 3). Compared to the decomposition results of dT_S/dQ_{AH}, the baseline contributions and surface temperature contributions for dT_2/dQ_{AH} are reduced, while contributions from atmospheric temperature are enhanced. The reason for the reduction of the baseline contribution can be explained by deriving $\partial T_2/\partial Q_{AH}$, as follows

$$\frac{\partial T_2}{\partial Q_{AH}} = \left(\frac{r_U - r_2}{r_U}\right)\frac{\partial T_S}{\partial Q_{AH}}. \tag{25}$$

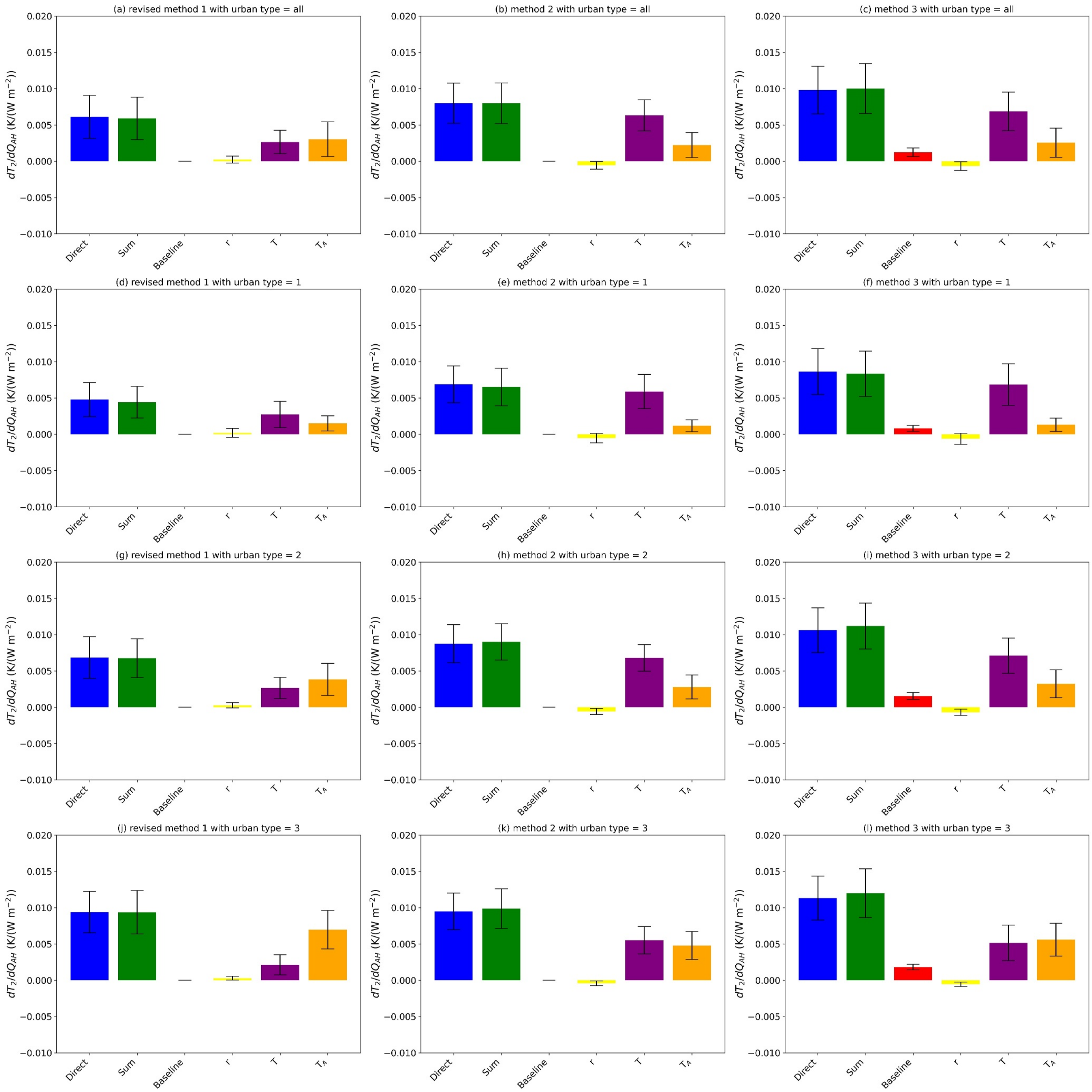

Figure 11. Decomposition of dT_2/dQ_{AH} (unit: K/(W m^{-2})) estimated with three Q_{AH} release methods for $\Delta Q_{AH} = 100$ W m^{-2}. From top to bottom: all urban types, urban type 1, urban type 2, urban type 3.

From Equation 25 one can see that $\partial T_2/\partial Q_{AH}$ differs from $\partial T_S/\partial Q_{AH}$ by a factor of $(r_U - r_2)/r_U$, which is smaller than unity. One can similarly show that the partial derivatives of T_2 with respect to key surface temperature variables (T_W and T_G) are smaller than their counterparts for T_S (again they differ by a factor of $(r_U - r_2)/r_U$, as shown in Supporting Information S1). The enhanced contributions from atmospheric temperature can be understood by comparing $\partial T_2/\partial T_A$ to $\partial T_S/\partial T_A$ (see Supporting Information S1). Intuitively, the schematic in Figure 2 makes it clear that compared to T_S, T_2 is influenced more strongly by T_A.

The examination of the partial derivatives (e.g., Equation 25) suggests that the baseline contributions to dT_2/dQ_{AH} would depend on urban types given that the baseline contributions to dT_S/dQ_{AH} depend on urban types. This is consistent with the results shown in Figure 11. The atmospheric contributions to dT_2/dQ_{AH} also show clear urban type dependence, which is similar to the results for dT_S/dQ_{AH}. However, the surface temperature contributions to dT_2/dQ_{AH} show no clear dependence on urban type (at least compared to their counterparts for dT_S/dQ_{AH}). This explains why overall the urban type dependence of dT_2/dQ_{AH} is weaker than that of dT_S/dQ_{AH} (cf., Figure 10 to Figure 8).

3.2.4. Structural Variants of SLUCM

Overall, dT_S/dQ_{AH} and dT_2/dQ_{AH} differ less across the three Q_{AH} release methods than dT_C/dQ_{AH}, but can still vary by as much as a factor of 4 for dT_S/dQ_{AH} and 2 for dT_2/dQ_{AH}. In this section, we examine the how dT_S/dQ_{AH} and dT_2/dQ_{AH} vary with the four SVs shown in Figure 1. Although dT_S/dQ_{AH} and dT_2/dQ_{AH} show dependence on urban types as shown earlier, their variations across the four SVs are similar for each urban type. Thus only the average results over all urban types are presented here.

As shown in Figure 12 and Table 2, dT_S/dQ_{AH} and dT_2/dQ_{AH} differ less across the four SVs compared to dT_C/dQ_{AH}. For dT_C/dQ_{AH}, changing the treatment of roof-air interaction and the parameterization of r_C can alter it by a factor of 4 (Figure 7) for method 3. However, for dT_S/dQ_{AH} and dT_2/dQ_{AH}, the differences are smaller (Figure 12), with the maximum difference of a factor of 2 for dT_2/dQ_{AH} between SV 2 (0.005 K/(W m^{-2})) and SV 3 (0.01 K/(W m^{-2})) with method 2.

The rankings of dT_S/dQ_{AH} and dT_2/dQ_{AH} across the four SVs are similar to each other, but are different from those of dT_C/dQ_{AH}. For dT_C/dQ_{AH}, their values are smaller in SVs 2 and 3 compared to those in SV 1, and hence their values in SV 4 are the smallest. However, for dT_S/dQ_{AH} and dT_2/dQ_{AH}, their values are reduced in SV 2 but more strongly increased in SV 3. Moreover, their values in SV 4 are more similar to those in SV 3 than those in SV 2, indicating that the parameterization of r_C has a stronger influence on dT_S/dQ_{AH} and dT_2/dQ_{AH} than the treatment of roof-air interaction.

Figures S8 and S9 in Supporting Information S1 examine the variations of dT_S/dQ_{AH} and dT_2/dQ_{AH}, respectively, across 4 different SVs with method 3. One feature of Figures S8 and S9 in Supporting Information S1 is that the baseline contributions consistently increase from SV 1 to SV 2 and from SV 1 to SV 3. As a result, SV 4 has the strongest baseline contributions for both dT_S/dQ_{AH} and dT_2/dQ_{AH}. These results are caused by the facts that (a) $\partial T_S/\partial Q_{AH}$ in SV 2 is always larger than $\partial T_S/\partial Q_{AH}$ in SV 1 (cf., Equation 23 to Equation 22), (b) $\partial T_S/\partial Q_{AH}$ increases with decreasing r_C (see Equation 22) and hence is larger in SV 3 than in SV 1, and (c) $\partial T_2/\partial Q_{AH}$ scales with $\partial T_S/\partial Q_{AH}$ (see Equation 25).

One can also show that $\partial T_S/\partial T_A$ becomes smaller in SV 3 than in SV 1 (see Supporting Information S1). This is consistent with how the contributions of atmospheric temperature to $\partial T_S/\partial Q_{AH}$ differ between SV 3 and SV 1 (cf. Figure S8c to Figure S8a in Supporting Information S1). However, contribution is the product of the partial derivative and the change of the contributing factor. Simply examining the partial derivative does not always provide the full picture (unless the change of the contributing factor is the same such as for baseline contributions where Q_{AH} is identical for all four SVs). For example, one can show that $\partial T_2/\partial T_A$ in SV 3 is smaller than in SV 1, yet the contribution of atmospheric temperature is actually higher in SV 3 than in SV 1 (cf. Figure S9c to Figure S9a in Supporting Information S1). This is because ΔT_A is stronger in SV 3 due to the enhanced Q_U as a result of smaller r_C.

Changes of contributions from surface temperatures and resistances do not show consistent patterns across the 4 SVs. This is partly because of the grouping of several surface temperatures (and resistances). The opposing changes within the group make it difficult to explain succinctly the combined changes.

4. Summary and Discussion

Using a suite of numerical simulations over the Greater Boston area conducted with WRF-SLUCM, the structural uncertainty associated with the sensitivity of urban temperatures to anthropogenic heat flux is quantified. In particular, we focus on how the sensitivity varies across three Q_{AH} release methods and four SV of SLUCM (Figure 1). These different methods of releasing Q_{AH} into the urban environment and SV of SLUCM are all credible model choices, meaning that none of them can be rejected based on our current understanding of urban-

Journal of Advances in Modeling Earth Systems

10.1029/2024MS004431

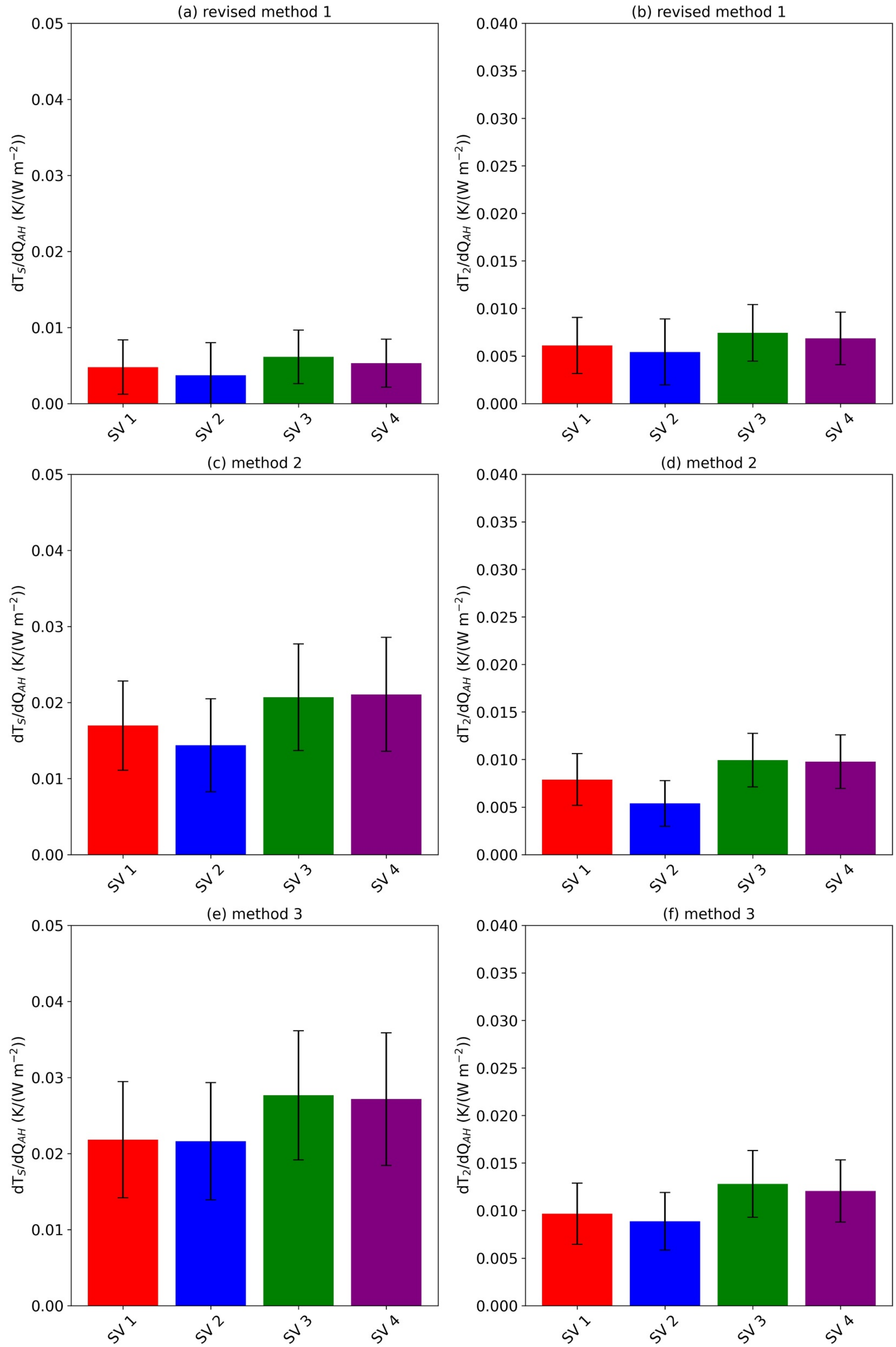

Figure 12. (a, c, e) dT_S/dQ_{AH} and (b, d, f) dT_2/dQ_{AH} across three Q_{AH} release methods and four different SVs (see Figure 1). These results are for $\Delta Q_{AH} = 100$ W m^{-2} and for all urban types.

atmosphere interaction and each of them can be found in the current generation of urban canopy models. Here we show that the sensitivity of urban canopy air temperature (T_C) to anthropogenic heat flux can differ by an order of magnitude across the three Q_{AH} release methods and by a factor of 4 across the four SV, highlighting the substantial structural uncertainty of dT_C/dQ_{AH}. The sensitivities of urban surface (T_S) and 2-m air (T_2) temperatures to anthropogenic heat flux are less affected by changing the Q_{AH} release method and the structure of SLUCM, but their sensitivities to anthropogenic heat flux can still vary by as much as a factor of 4 for surface temperature and 2 for 2-m air temperature.

It is important to discuss the implications and limitations of this work. First, understanding the structural uncertainty (as well as other uncertainties not examined here) associated with the sensitivity of urban temperatures to anthropogenic heat flux is important not only because this exercise yields insights into the physical processes controlling how urban temperatures respond to Q_{AH}, but also because these uncertainties provide some guidance as to how much uncertainty in the magnitude of Q_{AH} could be tolerated. The uncertainty in the magnitude of Q_{AH} is well recognized and research on quantifying/reducing such uncertainty should be encouraged. Nonetheless, it is important to realize that the uncertainty associated with the magnitude of Q_{AH} is only half of the story. Of equal importance is to quantify/reduce the uncertainty associated with the sensitivity. Along the same lines, while the scale dependence of Q_{AH} has long been recognized in the literature (Q_{AH} is a flux and almost by definition is scale-dependent), this work highlights that the sensitivity of urban temperatures to anthropogenic heat flux also depends on the scale at which the urban temperatures are defined, which may or may not be the same scale at which Q_{AH} is defined. Some thought experiment of matching the scales at which Q_{AH} and temperatures are defined can actually produce insights into the variability of dT/dQ_{AH}. For example, the canopy air temperature is implicitly defined over the canyon in SV 1 while it is defined over the entire impervious land in SV 2. Hence it is not surprising that $\partial T_C/\partial Q_{AH}$ in SV 2 is weaker than in SV 1. Similarly, Q_{AH} is defined over the impervious land in WRF-SLUCM while the surface temperature T_S and 2-m air temperature T_2 are defined over the grid cell. Hence the sensitivities of T_S and T_2 to Q_{AH} are highly dependent on the impervious surface fraction within the grid cell f_{urban} (the larger the f_{urban}, the higher these sensitivities).

Second, the large uncertainty associated with the WRF-SLUCM simulated dT/dQ_{AH} is fundamentally related to the challenges associated with simplifying complex urban environments in numerical models. In reality, Q_{AH} sources can exist at multiple levels within the urban canopy. Air conditioning and ventilation systems can release heat from any building floor levels, rooftops, or the ground. Additionally, heat emissions from vehicles and industrial processes add to the complexity of Q_{AH} source distribution. A recent study showed that the heat release location can have a strong impact on the simulated canopy air temperature and such impacts vary across seasons (L. Chen et al., 2024). This vertical variability of Q_{AH} source distribution justifies the three Q_{AH} release methods within the confines of SLUCM, but the vastly different dT/dQ_{AH} values in the three Q_{AH} release methods suggest potential benefits of employing more detailed descriptions of Q_{AH} sources. The vertical distribution of Q_{AH} sources could be used to inform the partition of Q_{AH} release in SLUCM (e.g., how much Q_{AH} should be released according to revised method 1 and how much should be released according to method 3). It can be also used with more sophisticated urban canopy models. One such model in WRF is the multi-layer UCM or BEP (Building Effect Parameterization) developed by Martilli et al. (2002). Unlike the SLUCM, the BEP recognizes that sources and sinks of heat, moisture, and momentum are distributed vertically throughout the entire urban canopy layer. While the current BEP in WRF does not directly use Q_{AH} as an input, it can incorporate Q_{AH} from air conditioning and ventilation at each building floor when coupled with a building energy model (BEM) (e.g., Salamanca et al., 2014; Takane et al., 2019). Therefore, using BEP-BEM can potentially better capture the vertical variability of Q_{AH} sources (at least from the building sector) and thus mitigate some of the structural uncertainties discussed in this study.

Third, this work examines various urban temperatures, including the canopy air temperature, surface temperature, and 2-m air temperature. Also examined are the roof surface temperature, the wall surface temperature, the canyon ground surface temperature, as well as the grass surface temperature. Adding Q_{AH} into the model tends to increase all these temperatures, yet their sensitivities to Q_{AH} differ. We do not, however, focus on the difference among different temperature variables in terms of their sensitivities to Q_{AH}, although such difference can be inferred from our results (e.g., in method 2 where Q_{AH} is released to the urban canyon ground the sensitivity of T_G is higher than the sensitivity of T_C, while in method 3 where Q_{AH} is released within the urban canyon the sensitivity of T_C is higher than the sensitivity of T_G). Instead, we focus on how the sensitivities of T_C, T_S, and T_2 vary across the three Q_{AH} release methods and the four SV. Among the three key temperatures examined here (T_C, T_S, and T_2), T_C tends to vary more strongly with Q_{AH} release methods and model SV than T_S and T_2. This work does not, however, address which temperature should be used as the golden metric to measure the effect of Q_{AH}. Nor does this work justify the current ways through which T_S and T_2 are diagnosed. Other methods of diagnosing T_S and T_2 within the WRF-SLUCM framework have been proposed elsewhere (Li & Bou-Zeid, 2014; Theeuwes et al., 2014) and different UCMs might have different ways of diagnosing T_S and T_2 (Qin et al., 2023). Moreover, it is not the purpose of this work to recommend whether, when, and where T_C or T_2 should be used if one was interested in studying urban air temperatures. Nonetheless, by clarifying the differences between T_C and T_2 (including their different sensitivities to Q_{AH}), this work might provide some insights as to how T_C and T_2, as well as their changes, should be interpreted. Similarly, this study does not provide justification to the current parameterizations for various resistances. The magnitude and variability of these resistances are not extensively discussed in this study, but it is clear that they are crucial in controlling the sensitivity of urban temperatures to Q_{AH} (e.g., see Equations 18, 19, 22, and 25). These resistances need to be improved as some of them are based on empirical relations derived from limited data or Monin-Obukhov similarity theory whose applicability over urban canopies is questionable.

Fourth, the goal of this work is not to simulate the realistic spatial/temporal patterns of the anthropogenic heat flux effect, which would require realistic spatial/temporal patterns of Q_{AH}. Instead, we focus on understanding the sensitivity of urban temperatures to Q_{AH}, or temperature changes per unit increase of Q_{AH}. Interestingly, the sensitivity does not vary strongly with the magnitude of Q_{AH} and seems to converge at large values of Q_{AH}, suggesting limited non-linearity in the response of urban temperatures to increasing Q_{AH}. This is good news for two reasons: (a) this implies that the number of physical processes controlling dT/dQ_{AH} is finite, (b) this opens the door for quantifying the effect of Q_{AH} through Equation 1 with a priori computed dT/dQ_{AH}. Further investigations on the variation of dT/dQ_{AH} with Q_{AH} are recommended to confirm these conjectures.

Fifth, this work only focuses on a 3-day summer period and the greater Boston area, and the analysis does not separate daytime from nighttime. These choices are motivated by the fact that the spatio-temporal variability has been investigated in a previous study (Wang et al., 2023) and is not the central focus of this work. Here we should note that the sensitivities of urban temperatures to Q_{AH} will change with meteorological/climatic conditions (e.g., wind speed, thermal stratification) and building parameters (which affect momentum and thermal roughness lengths). However, certain findings are robust such as the weaker $\partial T_C/\partial Q_{AH}$ in SV 2 than in SV 1, as demonstrated by comparing Equation 19 to Equation 18.

Lastly, although the study by Wang et al. (2023) and our work here demonstrate the spatio-temporal variability and structural uncertainty associated with dT/dQ_{AH}, it is perhaps equally important to provide a rule-of-thumb value for dT/dQ_{AH} for quick estimates. A good rule-of-thumb value for dT/dQ_{AH} is 0.01 K/(W m^{-2}), especially for T_2 (see Figure 12 and Table 2), which is consistent with previous literature (see the review by Wang et al. (2023)). Wang et al. (2023) provides some physical justification for this value (at least for T_C).

Acknowledgments

This research was supported by the U.S. Department of Energy, Office of Science, as part of research in MultiSector Dynamics, Earth and Environmental System Modeling Program. The work used resources of the National Energy Research Scientific Computing Center (NERSC), a U.S. Department of Energy Office of Science User Facility located at Lawrence Berkeley National Laboratory, operated under Contract No. DE-AC02-05CH11231. We also acknowledge the high-performance computing support from Cheyenne (https://doi.org/10.5065/D6RX99HX) and Derecho (https://doi.org/10.5065/qx9a-pg09) provided by NCAR's Computational and Information Systems Laboratory, sponsored by the National Science Foundation. DL acknowledges support from the U.S. National Science Foundation (NSF-ICER-1854706). TS is supported by UKRI NERC Independent Research Fellowship (NE/P018637/2). The authors thank Dr. Cenlin He at National Center for Atmospheric Research (NCAR) for constructive discussions and also thank the reviewers whose comments helped improve the paper.

Data Availability Statement

The WRF outputs of this work were produced with a modified version of WRF v4.2.2 (Li, 2024a). The scripts to reproduce the figures are archived as Li (2024b).

References

Allen, L., Lindberg, F., & Grimmond, C. (2011). Global to city scale urban anthropogenic heat flux: Model and variability. *International Journal of Climatology*, *31*(13), 1990–2005. https://doi.org/10.1002/joc.2210

Bohnenstengel, S., Hamilton, I., Davies, M., & Belcher, S. (2014). Impact of anthropogenic heat emissions on London's temperatures. *Quarterly Journal of the Royal Meteorological Society*, *140*(679), 687–698. https://doi.org/10.1002/qj.2144

Brutsaert, W. (1982). *Evaporation into the atmosphere: Theory, history and applications* (Vol. 1). Springer Science & Business Media.

Chehbouni, A., Seen, D. L., Njoku, E., & Monteny, B. (1996). Examination of the difference between radiative and aerodynamic surface temperatures over sparsely vegetated surfaces. *Remote Sensing of Environment*, *58*(2), 177–186. https://doi.org/10.1016/s0034-4257(96)00037-5

Chen, F., Kusaka, H., Bornstein, R., Ching, J., Grimmond, C., Grossman-Clarke, S., et al. (2011). The integrated WRF/urban modelling system: Development, evaluation, and applications to urban environmental problems. *International Journal of Climatology*, *31*(2), 273–288. https://doi.org/10.1002/joc.2158

Chen, F., Yang, X., & Wu, J. (2016). Simulation of the urban climate in a Chinese megacity with spatially heterogeneous anthropogenic heat data. *Journal of Geophysical Research: Atmospheres*, *121*(10), 5193–5212. https://doi.org/10.1002/2015jd024642

Chen, L., Yang, J., & Zheng, X. (2024). Modelling the impact of building energy consumption on urban thermal environment: The bias of the inventory approach. *Urban Climate*, *53*, 101802. https://doi.org/10.1016/j.uclim.2023.101802

Dong, Y., Varquez, A., & Kanda, M. (2017). Global anthropogenic heat flux database with high spatial resolution. *Atmospheric Environment*, *150*, 276–294. https://doi.org/10.1016/j.atmosenv.2016.11.040

Dudhia, J. (1989). Numerical study of convection observed during the winter monsoon experiment using a mesoscale two-dimensional model. *Journal of the Atmospheric Sciences*, *46*(20), 3077–3107. https://doi.org/10.1175/1520-0469(1989)046⟨3077:nsocod⟩2.0.co;2

Hong, S.-Y. (2010). A new stable boundary-layer mixing scheme and its impact on the simulated East Asian summer monsoon. *Quarterly Journal of the Royal Meteorological Society*, *136*(651), 1481–1496. https://doi.org/10.1002/qj.665

Hong, S. Y., Lim, K. S., Kim, J. H., & Lim, J. O. (2006). The WRF single-moment-microphysics scheme class 6 (WSM6). *Asia-Pacific Journal of Atmospheric Sciences*, *42*, 129–151.

Hong, S.-Y., Noh, Y., & Dudhia, J. (2006). A new vertical diffusion package with an explicit treatment of entrainment processes. *Monthly Weather Review*, *134*(9), 2318–2341. https://doi.org/10.1175/mwr3199.1

Kusaka, H., Kondo, H., Kikegawa, Y., & Kimura, F. (2001). A simple single-layer urban canopy model for atmospheric models: Comparison with multi-layer and slab models. *Boundary-Layer Meteorology*, *101*(3), 329–358. https://doi.org/10.1023/a:1019207923078

Kustas, W. P., Choudhury, B. J., Moran, M. S., Reginato, R. J., Jackson, R. D., Gay, L. W., & Weaver, H. L. (1989). Determination of sensible heat flux over sparse canopy using thermal infrared data. *Agricultural and Forest Meteorology*, *44*(3–4), 197–216. https://doi.org/10.1016/0168-1923(89)90017-8

Lemonsu, A., Grimmond, C., & Masson, V. (2004). Modeling the surface energy balance of the core of an old Mediterranean city: Marseille. *Journal of Applied Meteorology and Climatology*, *43*(2), 312–327. https://doi.org/10.1175/1520-0450(2004)043<0312:mtsebo>2.0.co;2

Li, D. (2024a). Modified WRF v4.2.2 for Li 2024 JAMES WRF AH [Software]. *Zenodo*. https://doi.org/10.5281/zenodo.13259039

Li, D. (2024b). Scripts for Li 2024 JAMES WRF AH [Dataset]. *Zenodo*. https://doi.org/10.5281/zenodo.11099555

Li, D., & Bou-Zeid, E. (2014). Quality and sensitivity of high-resolution numerical simulation of urban heat islands. *Environmental Research Letters*, *9*(5), 055001. https://doi.org/10.1088/1748-9326/9/5/055001

Li, D., Bou-Zeid, E., Barlage, M., Chen, F., & Smith, J. A. (2013). Development and evaluation of a mosaic approach in the WRF-NOAH framework. *Journal of Geophysical Research: Atmospheres*, *118*(21), 11–918. https://doi.org/10.1002/2013jd020657

Li, D., Malyshev, S., & Shevliakova, E. (2016a). Exploring historical and future urban climate in the Earth system modeling framework: 1. Model development and evaluation. *Journal of Advances in Modeling Earth Systems*, *8*(2), 917–935. https://doi.org/10.1002/2015ms000578

Li, D., Malyshev, S., & Shevliakova, E. (2016b). Exploring historical and future urban climate in the Earth system modeling framework: 2. Impact of urban land use over the continental United States. *Journal of Advances in Modeling Earth Systems*, *8*(2), 936–953. https://doi.org/10.1002/2015ms000579

Lipson, M. J., Grimmond, S., Best, M., Abramowitz, G., Coutts, A., Tapper, N., et al. (2024). Evaluation of 30 urban land surface models in the urban-plumber project: Phase 1 results. *Quarterly Journal of the Royal Meteorological Society*, *150*(758), 126–169. https://doi.org/10.1002/qj.4589

Luo, X., Vahmani, P., Hong, T., & Jones, A. (2020). City-scale building anthropogenic heating during heat waves. *Atmosphere*, *11*(11), 1206. https://doi.org/10.3390/atmos11111206

Martilli, A., Clappier, A., & Rotach, M. W. (2002). An urban surface exchange parameterisation for mesoscale models. *Boundary-Layer Meteorology*, *104*(2), 261–304. https://doi.org/10.1023/a:1016099921195

Masson, V. (2000). A physically-based scheme for the urban energy budget in atmospheric models. *Boundary-Layer Meteorology*, *94*(3), 357–397. https://doi.org/10.1023/a:1002463829265

Mesinger, F., DiMego, G., Kalnay, E., Mitchell, K., Shafran, P. C., Ebisuzaki, W., et al. (2006). North American regional reanalysis. *Bulletin of the American Meteorological Society*, *87*(3), 343–360. https://doi.org/10.1175/bams-87-3-343

Mlawer, E. J., Taubman, S. J., Brown, P. D., Iacono, M. J., & Clough, S. A. (1997). Radiative transfer for inhomogeneous atmospheres: RRTM, a validated correlated-k model for the longwave. *Journal of Geophysical Research*, *102*(D14), 16663–16682. https://doi.org/10.1029/97jd00237

Monin, A., & Obukhov, A. (1954). Basic laws of turbulent mixing in the ground layer of the atmosphere. *Trudy Instituta Geologicheskikh Nauk Akademii Nauk SSSR*, *151*, 163–187.

Monteith, J., & Unsworth, M. (2013). *Principles of environmental physics: Plants, animals, and the atmosphere*. Academic Press.

Oke, T. R., Mills, G., Christen, A., & Voogt, J. A. (2017). *Urban climates*. Cambridge University Press.

Oleson, K. W., Bonan, G. B., Feddema, J., Vertenstein, M., & Grimmond, C. (2008). An urban parameterization for a global climate model. Part I: Formulation and evaluation for two cities. *Journal of Applied Meteorology and Climatology*, *47*(4), 1038–1060. https://doi.org/10.1175/2007jamc1597.1

Oleson, K. W., & Feddema, J. (2020). Parameterization and surface data improvements and new capabilities for the Community Land Model Urban (CLMU). *Journal of Advances in Modeling Earth Systems*, *12*(2), e2018MS001586. https://doi.org/10.1029/2018ms001586

Oleson, K. W., Lawrence, D. M., Bonan, G., Drewniak, B., Huang, M., Koven, C., et al. (2010). Technical description of version 4.0 of the Community Land Model (CLM). *NCAR Technical Note NCAR/TN-478+ STR* (Vol. *257*, pp. 1–257).

Qin, Y., Liao, W., & Li, D. (2023). Attributing the urban–rural contrast of heat stress simulated by a global model. *Journal of Climate*, *36*(6), 1805–1822. https://doi.org/10.1175/jcli-d-22-0436.1

Sailor, D. J. (2011). A review of methods for estimating anthropogenic heat and moisture emissions in the urban environment. *International Journal of Climatology*, *31*(2), 189–199. https://doi.org/10.1002/joc.2106

Sailor, D. J., Georgescu, M., Milne, J. M., & Hart, M. A. (2015). Development of a national anthropogenic heating database with an extrapolation for international cities. *Atmospheric Environment*, *118*, 7–18. https://doi.org/10.1016/j.atmosenv.2015.07.016

Salamanca, F., Georgescu, M., Mahalov, A., Moustaoui, M., & Wang, M. (2014). Anthropogenic heating of the urban environment due to air conditioning. *Journal of Geophysical Research: Atmospheres*, *119*(10), 5949–5965. https://doi.org/10.1002/2013jd021225

Skamarock, W. C., Klemp, J. B., Dudhia, J., Gill, D. O., Liu, Z., Berner, J., et al. (2019). A description of the advanced research WRF version 4. *NCAR Technical Note NCAR/TN-556+ STR* (p. 145).

Stensrud, D. J. (2009). *Parameterization schemes: Keys to understanding numerical weather prediction models*. Cambridge University Press.

Takane, Y., Kikegawa, Y., Hara, M., & Grimmond, C. S. B. (2019). Urban warming and future air-conditioning use in an Asian megacity: Importance of positive feedback. *npj Climate and Atmospheric Science*, *2*(1), 39. https://doi.org/10.1038/s41612-019-0096-2

Theeuwes, N., Steeneveld, G., Ronda, R., Heusinkveld, B., Van Hove, L., & Holtslag, A. (2014). Seasonal dependence of the urban heat island on the street canyon aspect ratio. *Quarterly Journal of the Royal Meteorological Society*, *140*(684), 2197–2210. https://doi.org/10.1002/qj.2289

Thom, A. (1972). Momentum, mass and heat exchange of vegetation. *Quarterly Journal of the Royal Meteorological Society*, *98*(415), 124–134. https://doi.org/10.1256/smsqj.41509

Troufleau, D., Lhomme, J.-P., Monteny, B., & Vidal, A. (1997). Sensible heat flux and radiometric surface temperature over sparse Sahelian vegetation. I. An experimental analysis of the kB^{-1} parameter. *Journal of Hydrology*, *188*, 815–838. https://doi.org/10.1016/s0022-1694(96)03172-1

Vahmani, P., Luo, X., Jones, A., & Hong, T. (2022). Anthropogenic heating of the urban environment: An investigation of feedback dynamics between urban micro-climate and decomposed anthropogenic heating from buildings. *Building and Environment*, *213*, 108841. https://doi.org/10.1016/j.buildenv.2022.108841

Varquez, A. C. G., Kiyomoto, S., Khanh, D. N., & Kanda, M. (2021). Global 1-km present and future hourly anthropogenic heat flux. *Scientific Data*, *8*(1), 64. https://doi.org/10.1038/s41597-021-00850-w

Wang, L., Sun, T., Zhou, W., Liu, M., & Li, D. (2023). Deciphering the sensitivity of urban canopy air temperature to anthropogenic heat flux with a forcing-feedback framework. *Environmental Research Letters*, *18*(9), 094005. https://doi.org/10.1088/1748-9326/ace7e0

Yang, B., Yang, X., Leung, L. R., Zhong, S., Qian, Y., Zhao, C., et al. (2019). Modeling the impacts of urbanization on summer thermal comfort: The role of urban land use and anthropogenic heat. *Journal of Geophysical Research: Atmospheres*, *124*(13), 6681–6697. https://doi.org/10.1029/2018jd029829

Zhou, W., Wang, L., Li, D., & Leung, L. R. (2021). Spatial pattern of lake evaporation increases under global warming linked to regional hydroclimate change. *Communications Earth & Environment*, *2*(1), 255. https://doi.org/10.1038/s43247-021-00327-z